PLASMA DIAGNOSTICS AND ITO FILM DEPOSITION BY RF-ASSISTED CLOSED-FIELD DUAL MAGNETRON SYSTEM

BY

LIANG MENG

THESIS

Submitted in partial fulfillment of the requirements
for the degree of Master of Science in Nuclear Engineering
in the Graduate College of the
University of Illinois at Urbana-Champaign, 2010

Urbana, Illinois

Adviser:

Professor David N. Ruzic, Chair
Professor George H. Miley

PLASMA DIAGNOSTICS AND ITO FILM DEPOSITION BY RF-ASSISTED CLOSED-FIELD DUAL MAGNETRON SYSTEM

Liang Meng
Department of Nuclear, Plasma, and Radiological Engineering
University of Illinois at Urbana-Champaign, 2010
David N. Ruzic, Adviser

Deposition of indium tin oxide (ITO) among various transparent conductive materials on flexible organic substrates has been intensively investigated among academics and industrials for a whole new array of imaginative optoelectronic products. One critical challenge coming with the organic materials is their poor thermal endurances, considering that the process currently used to produce industry-standard ITO usually involves relatively high substrate temperature in excess of 200℃ and post-annealing. A lower processing temperature is thus demanded, among other desires of high deposition rate, large substrate area, good uniformity, and high quality of the deposited materials.

For this purpose, we developed an RF-assisted closed-field dual magnetron sputtering system. The "prototype" system consists of a 3-inch unbalanced dual magnetron operated at a closed-field configuration. An RF coil was fabricated and placed between the two magnetron cathodes to initiate a secondary plasma. The concept is to increase the ionization faction with the RF enhancement and utilize the ion energy instead of thermal energy to facilitate the ITO film growth. The closed-field unbalanced magnetrons create a plasma in the intervening region rather than confine it near the target, thus achieving a large-area processing capability.

An RF-compensated Langmuir probe was used to characterize and compare the plasmas in mirrored balanced and closed-field unbalanced magnetron configurations. The spatial distributions of the electron density n_e and electron temperature T_e were measured. The density profiles reflect the shapes of the plasma. Rather than intensively concentrated to the targets/cathodes in the balanced magnetrons, the plasma is more dispersive in the closed-field mode with a twice higher electron density in the substrate region. The RF assistance significantly enhances n_e by one or two orders of magnitude higher. The effect of various

other parameters, such as pressure, on the plasma was also studied.

The ionization fractions of the sputtered atoms were measured using a gridded energy analyzer (GEA) combined with a quartz crystal microbalance (QCM). The presence of the RF plasma effectively increases the ITO ionization fraction to around 80% in both the balanced and closed-field unbalanced configurations. The ionization fraction also varies with pressure, maximizing at 5-10 mTorr. The study of the ionization not only facilitates understanding the plasma behaviors in the RF-assisted magnetron sputtering, but also provides a criterion for optimizing the film deposition process.

ITO films were deposited on both glass and plastic (PET) substrates in the 3-inch RF-assisted closed-field magnetrons. The electrical resistivity and optical transmission transparency of the ITO films were measured. Appropriate RF assistance was shown to dramatically reduce the electrical resistivity. An ITO film with a resistivity of 1.2×10^{-3} Ω-cm and a visible light transmittance of 91% was obtained with a 225 W RF enhancement, while the substrate temperature was monitored as below 110 ℃. X-ray photoelectron spectroscopy (XPS) was employed to confirm the ITO film stoichiometry. The surface morphology of the ITO films and its effect on the film properties were studied using atomic force microscopy (AFM). The prototype of RF-assisted closed-field magnetron was further extended to a larger rectangular shaped dual magnetron in a flat panel display manufacturing system. Similar improvement of the ITO film conductivities by the auxiliary RF was observed on the large-area PET substrates. Meanwhile, significant deposition rates of 25-42 nm/min were achieved.

ACKNOWLEDGEMENTS

First, I would like to thank my adviser, Professor David N. Ruzic. He has completely supported and guided me over the last three years of graduate school. He is a constant source of knowledge and always provides different innovative ideas for the experiments. I learned my first knowledge of plasma diagnostics from him and am guided to learn more from different research topics. I would say I like the engineering because of his instructions. He is also a friend, consistently encouraging me to get used to the American life and helping me prepare for the future career. I am really glad that I was admitted by UIUC when I applied for the graduate school three years ago, and have this chance to work with Prof. Ruzic.

I would like to thank my thesis reader, Professor George H. Miley. I took several classes from him, Plasma and Fusion Science, and Plasma engineering. I did learn a lot from these lessons, even though it's really difficult to really follow his deep thoughts. Prof. Miley gives me a lot of suggestions for my thesis writing and they are really intelligent.

Prof. Angus Rockett from the Department of Materials Science and Engineering is greatly acknowledged. As the new President-Elect of the AVS Science and Technology Society, he is a guru in the photovoltaic materials. He has kindly given many insightful suggestions for the work. And I've learned an important lesson from him regarding the strictness and passion in the scientific research, which will benefit my entire career. He is also thanked for generously sharing some of his equipments, based on which the experimental chamber employed in this work was constructed.

I also need to thank Tom Dockstader from Kurt J. Lesker Company. We collaborated with him for this research work and part of the experiments were done using their device. He was kind and willing to help with different problems we encountered. His expertise on the transparent conductive materials was crucial for the entire work.

The post-docs and graduate students working under Prof. Ruzic, the Center of Plamsa-Material Interactions (CPMI), have always been friendly and helpful. Dr. Carlos Henry Castano was my first mentor in the CPMI. He always quickly responded to all my questions and showed me the best ways to solve different problems. He helped me quickly adapt to the graduate research and change from a physics student into an engineering one. Dr. Ramasamy Raju had worked together with me on this project and gave me all his supports. He not only shared his intelligent ideas but also helped me do all the heavy liftings. Dr. Randolph Flauta, was very generous to assist me writing the papers and proposals on this project. I really benefit a lot due to his broad knowledge from many years' working experiences in industries. Dr. Martin J. Neumann, was more like a advisor. He was an invaluable source and was actually managing the lab for a long while. He was keen and yet strict with all the researches. My only fear is I did not exploit his knowledge as much as I should have. Current CPMI members Wayne Lyte, Eithan Ritz, John Sporre have taught me more than they probably realize. Special thanks to my friend, Dr. Hyungjoo Shin. He was three years senior than me and was so generous, smart and diligent. Because of these, he was always the one I turned to with all kinds of questions.

And finally, I would like to thank my family. My parents and brother have been consistently supporting me for my study, especially abroad. I owe them in the completion of my college, my thesis here, as everything else. For my wife, I don't need too many words. Just, thank you, for being by my side.

Table of Contents

Chapter 1 Introduction and Motivation

Indium tin oxide (ITO), among various transparent conductive materials, is essential for a variety of optoelectronic device applications from organic light emitting diodes (OLED) to flat panel displays. Magnetron sputtering is a common method to produce thin ITO films. However, the demands for displays of larger area flexible organic substrates present new challenges as to lower the processing temperature as well as to improve the deposition uniformity. We proposed a new method of closed-field magnetron sputtering with RF enhancement for this purpose. The RF assistance is used to increase the plasma density and enhance the ionization of the sputtered materials. Energy is thus added to the growing films by ion bombardments instead of the substrate heating. High-quality ITO films (i.e., of low electrical resistivity and high optical transparency) are expected without using substrate heating or post-annealing. Plasma diagnostics and ITO film characterizations were performed to confirm the improvements in both plasma parameters and film properties.

1.1 Indium Tin Oxide

The electronics industry has undergone a renaissance in the past decade as the flat panel plasma displays become a more affordable consumer product. Displays continue to be manufactured larger and larger as the demand increases. The ability to make inexpensive flexible plasma displays on plastic (or other organic) substrates can usher in a new generation of products.

Transparent conductive materials are essential for such applications. They traditionally act as the electrodes for injection of charge carriers as well as allowing the emitted light to pass through with very low losses. Although a partial transparency, with an acceptable reduction in conductivity, can be obtained for very thin metallic films, high transparency and simultaneously high conductivity cannot be attained in intrinsic stoichiometric materials. The only way this can be achieved is by creating electron

degeneracy in a wide band gap (E_g > 3eV or more for visible radiations) material by controllably introducing non-stoichiometry and/or appropriate dopants. These conditions can be easily met for indium tin oxide (ITO) as well as a number of other transparent conductive oxide (TCO) materials.

ITO is a highly degenerate semiconductor, i.e. it has so many dopants that the electron concentration in the conduction band or hole concentration in the valence band is comparable with the density of states in the band. The degeneracy is caused by both oxygen vacancies and substitutional tin dopants created during the film growth. [1]

ITO has already been used in a variety of consumer electronic applications, and is continuously being studied extensively for more optoelectronic device applications such as organic light emitting diodes (OLEDs) [2], solar cells [3], liquid crystal displays (LCDs) [4] and plasma display panels (PDPs) [5]. These types of applications require varying many process parameters to maximize the transmission of light as well as to keep the resistivity of the film low. ITO, with the reported superior transmittance and conductivity as high as 95% and 10^4 $\Omega^{-1}cm^{-1}$ respectively, is among the most popular TCO thin films. Typically glass substrates are used but the shift to the organic substrates is now under intensive investigation [6,7] as the demand for large area flexible displays on plastic or other organic substrates is growing.

To produce industry-standard TCO (i.e. with a visible light transmission higher than 90% of and a resistivity of $1x10^{-4}$ Ohm-cm or lower), it usually involves deposition at relatively high substrate temperature in excess of 200℃ which increases further when annealing treatments are made on the films [8-12]. For the growth of ITO films onto the organic substrates with quite poor thermal endurance, however, it is necessary to control the substrate temperature below 150 ℃.

Various techniques have been used to grow ITO films, including chemical vapor

deposition [13], evaporation deposition [14], magnetron sputtering [15], spray pyrolysis [16], ion-assisted deposition [17], and laser-assisted deposition techniques [18]. The DC magnetron sputtering technique, with an ability to produce high quality films at relatively higher deposition rates has been commonly used to prepare ITO thin films.

In order to reduce the processing temperature, different ways to add energy to the growing TCO films instead of heating the substrate have been tried, such as ion-assisted deposition [19,20], ion beam sputtering [21,22] and pulsed-laser deposition [23]. In these methods, the bombardment of energetic ions and atoms can improve the electrical and optical property of the TCO film by efficiently transferring their kinetic energy to the surface adatoms and in turn, modifying surface morphology [24]. However, there is a concern that energetic ion radiation can cause damage to organic materials and result in degraded device performance [25]. Also the above methods are typically limited to a low pressure operation with a low deposition rate, making them difficult to be adapted to a large-area deposition. A plasma-assisted magnetron sputtering has also been reported to fabricate TCO films at a low temperature [26]. More ions are created by the secondary plasma assistance and potentially provide an efficient energy transfer to the growing films. Since the sputtering can produce smoother and denser films, there is great motivation to combine the plasma assistance with the magnetron sputtering. In view of this, a new RF plasma-assisted closed-field dual magnetron sputtering system was proposed and developed. The enhancement of ionization by RF assistance and its effect on the ITO film deposition were studied.

1.2 Magnetron Sputtering Configuration

Magnetron sputtering has been widely used in the manufacture of industrial coatings. It offers a flexible deposition process with high throughput and can be used for high-purity thin film fabrication in semiconductors or for large-area coatings of structural materials such as the glass windows. One of the main advantages of magnetron sputtering over the other competing physical vapor deposition techniques is the additional kinetic energy of the sputtered atoms. This kinetic energy can lead to a more adherent coating and better conformal coverage. It also benefits the formation of many different compound thin films at much lower temperature, which is a great advantage when the temperature-sensitive substrates are used [27,28].

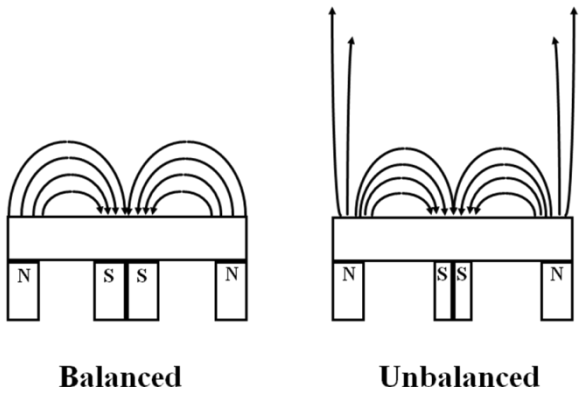

Figure 1.1 Examples of balanced and unbalanced magnetron systems.

A magnetron can be run in a variety of ways for different applications. In many cases, the magnetron is run "balanced". In this mode, the magnetic field strength of all the magnets is set such that the field lines all remain in closed loops, running from one magnet to another, as illustrated in Figure 1.1. In other words, the magnetic field lines emanating from the inner magnet(s) all end on the outer magnets, and vice versa. Such a configuration results in the best confinement of electrons. Thus the feed gas can be strongly ionized to give a high sputtering rate. However this confinement tends to prevent the plasma from spreading. In contrast to the balanced magnetron, an "unbalanced" magnetron specifically allows the field lines to end on the surfaces other than the permanent magnets (referring to Figure 1.1). Depending upon how unbalanced the magnetron is, a small or large portion of the electrons

may escape and travel away from the magnetron. As a result, the sputtering rate is reduced. However, the plasma extends further away from the magnetron surface. This is useful in various situations.

The configurations become more interesting when two or more magnetrons are used in conjunction. One of the more recent developments in magnetron system is the use a dual magnetron sputtering system in a balanced "mirrored" configuration or an unbalanced "closed-field" configuration [29], as shown respectively in Figure 1.2. If two balanced magnetrons are brought together facing each other, they will produce what is known as a "mirrored" configuration. This is very useful in cases that each magnetron is sputtering a different material, and the region between the magnetrons is used for deposition/reaction.

In a "closed-field" configuration, each of the two magnetrons is run effectively unbalanced alone, but the dual magnetron pair is balanced as a group. To produce such a configuration, the magnetic field polarity of one magnetron is flipped so that the south becomes north and vice versa. A significant plasma is extended to the intervening region between the two magnetron cathodes and maintained there [30].

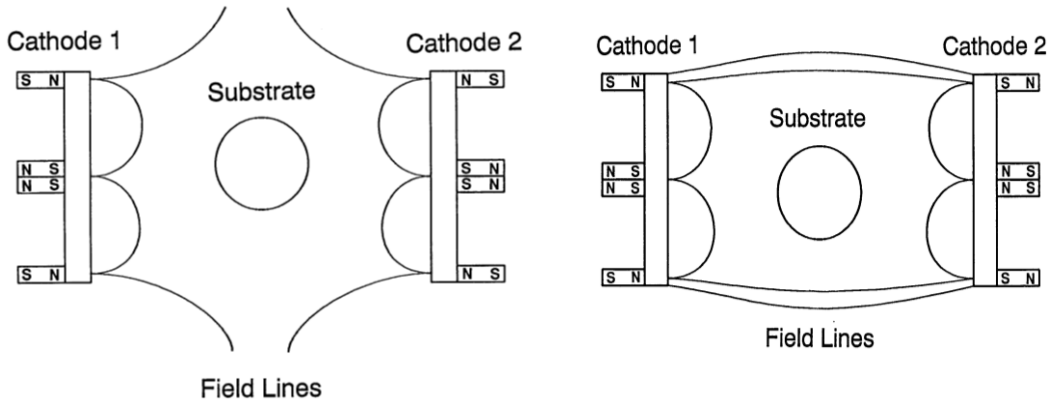

Figure 1.2 Dual magnetron configurations: mirrored (left) and closed-field (right) systems.

1.3 Ionized Physical Vapor Deposition

As stated previously, the processing temperature for the ITO film fabrication needs to be reduced, and the ion assistance is a promising way to add energy to the growing films without heating up the substrate excessively. Ionized physical vapor deposition (iPVD) has been developed as a high plasma density tool to increase the ion flux. An iPVD essentially consists following steps: 1) creating a metal vapor flux by physical methods, such as the sputtering and evaporation; 2) ionizing the metal neutral using a high density secondary plasma source or a single enhanced ionization source; 3) collimating the ion flux by the plasma sheath or negative bias before deposition [31]. The iPVD has been widely utilized in the integrated circuit (IC) manufacturing as the primary approach for Cu barrier/seed layer deposition in the interconnects [32]. Comparing with the conventional PVD, iPVD significantly improves the bottom and sidewall coverage in the trenches and vias [33-35].

A typical iPVD system involves a DC (or RF) magnetron, and a secondary high density plasma, which is commonly an inductively coupled plasma (ICP) or an electron cyclotron resonance (ECR) plasma [36-39]. In some tools, a single source can be used for both sputtering and ionizing the target material, such as the hollow cathode magnetron (HCM) [40].

In this study, we proposed and investigated the incorporation of an RF coil in a closed-field magnetron sputtering system as the secondary ionization source. The coil was placed between the magnetron pair in order to excite a secondary plasma near the targets and create more ionizations of the sputtered atoms (Figure 1.3). The combination of the RF coil and the closed-field magnetron configuration should produce a denser and more uniform plasma extended to the substrate region, providing more flexibilities in the sputtering process.

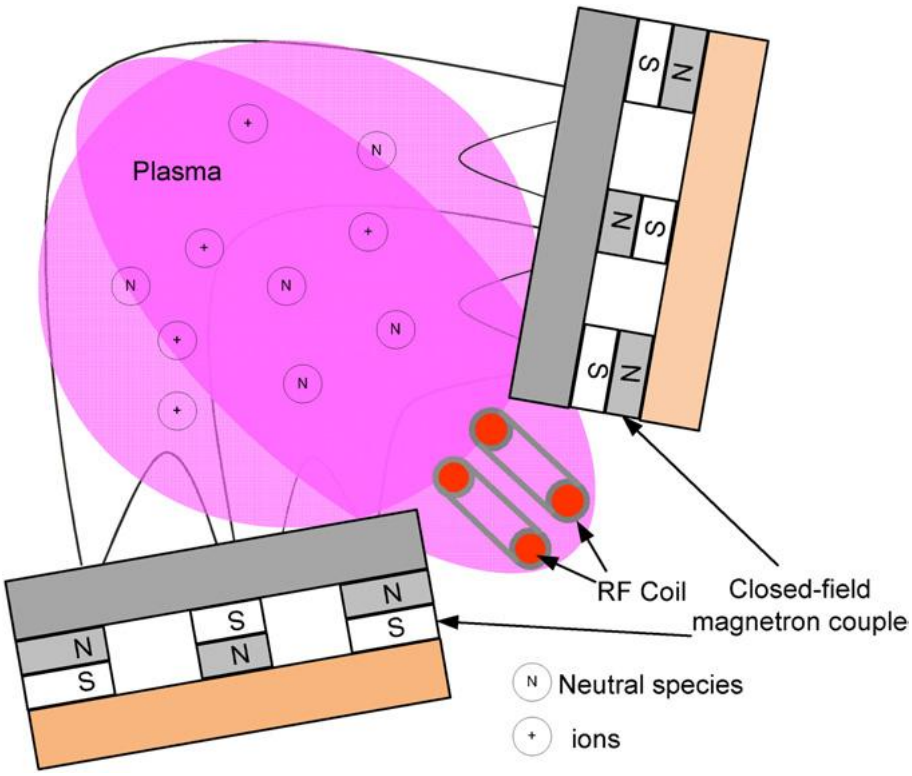

Figure 1.3 Schematic diagram of an unbalanced "closed-field" magnetron sputtering setup.

1.4 Objective

There is considerable motivation to combine the plasma assistance with the closed-field dual magnetron as already mentioned. It is not only suitable for the low temperature fabrication of good TCO films but is also easy to achieve high deposition rate and be scaled up to a large-area deposition (e.g. roll-to-roll process).

In this thesis, a prototype of RF plasma-assisted closed-field magnetron sputtering system was designed and tested. The closed-field unbalanced configuration was compared with the balanced configuration. 3-D Langmuir probe diagnostics were performed to better depict the plasma confinement in these two configurations. The influence of the RF enhancement, along with the other process parameters, on the spatial distribution of the electron density and electron temperature were studied. One of the most important properties, the ionization fraction of sputtered materials, was measured using a quartz crystal microbalance (QCM) and a gridded energy analyzer (GEA). The study of the ionization provides more insight into the effects of the magnetron configuration and the RF assistance. The system was tested for thin ITO film deposition without substrate heating. The improvement of film properties by the system, especially by varied auxiliary RF power, was explored. Finally, I modified the prototype system and scaled it up to a larger linear dual-magnetron for use in an industrial flat panel display manufacturing system. The ITO film deposition study was repeated using this test bed. This part of work was in collaboration with Kurt J. Lesker Company.

Chapter 2 Experimental Setup

In this chapter, a new RF-enhanced closed-field magnetron sputtering deposition system is described, in terms of its design, construction and installation. Various experiments were performed in this system to test its suitability for ITO film deposition. The plasma diagnostics used a 3-D scanning RF-compensated Langmuir probe. The details of the setup and related background information are introduced. Ionization fraction measurements were performed employing a gridded energy analyzer (GEA) combined with a quartz crystal microbalance (QCM). The concept of this tool and its specific design are described. Finally, the system configuration for the ITO film deposition and the experimental procedures employed are presented.

2.1 Magnetron Sputtering Deposition System

2.1.1 Dual magnetron sputtering system – SHADE

The majority of the experiments were done at the Center of Material and Plasma Interactions (CMPI), UIUC. The tool employed was a dual magnetron sputtering system – "SHADE (Sputtering High-purity Atomic Deposition Experiment)" as shown in Figure 2.1, along with a schematic diagram shown in Figure 2.2. The system consists of a main cylindrical chamber of 9 inches in diameter and 19 inches in length, and different units such as vacuum, gas controlling, dual magnetron, secondary RF coil, substrate, sample loading and water cooling system. A second loadlock chamber is used for sample transfer. Professor Angus Rockett [41] is gratefully acknowledged for his courtesy of donating the chamber.

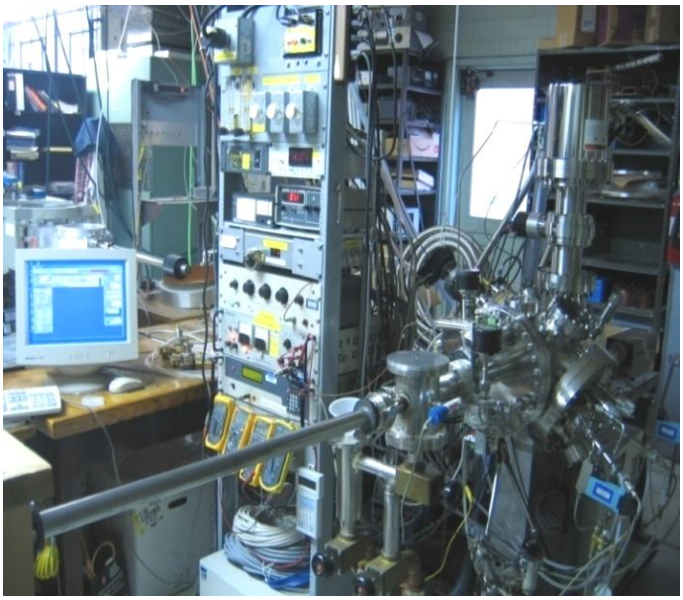

Figure 2.1 Dual magnetron sputtering system – SHADE

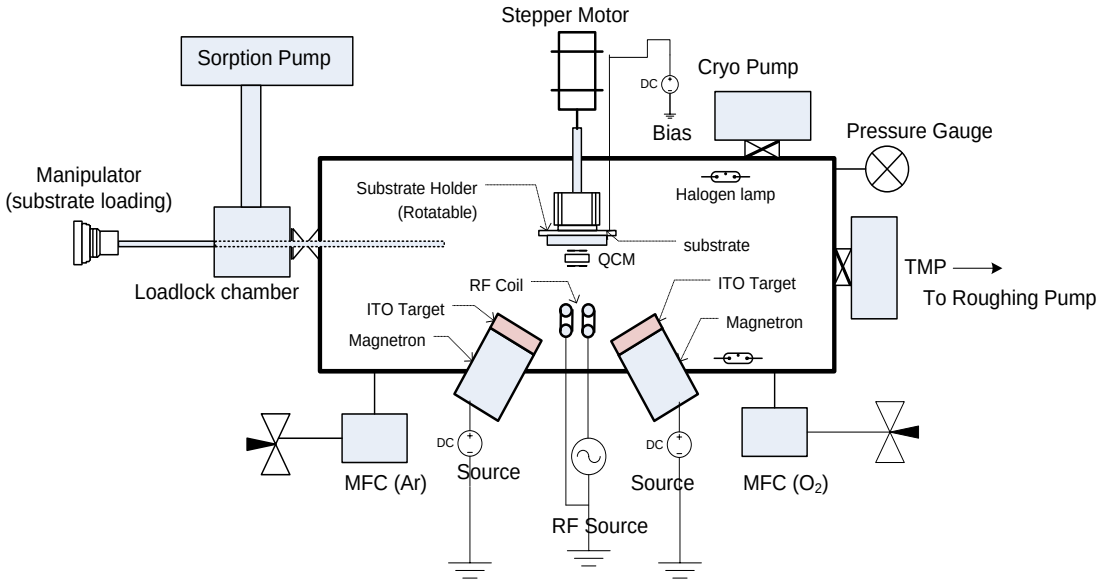

Figure 2.2 Schematic diagram of the RF-assisted dual magnetron sputtering system – SHADE.

The vacuum system for the main chamber includes a turbo molecular pump (TMP) followed by a roughing pump and a cryo pump to obtain a base pressure as low as 10^{-8} Torr. Halogen lamps are used to bake out the chamber. The gas pressure is monitored with a combination of different gauges, e. g. Convectron, Baratron and ion gauges. Ultra high purity Ar gas was used for the all the experiments for the plasma diagnostics and film deposition. A small amount of O_2 was added in the ITO film deposition process. The gases are injected

through needle valves and their flow rates are controlled by two mass flow controllers respectively. The working pressure was adjusted between 1 to 40 mTorr during experiments, as read from the Baratron gauge.

In this study, two different sets of magnetrons were used. Figure 2.3 shows (a) the 2-inch and (b) the 3-inch dual magnetron pair. The 2-inch magnetrons using metal targets such as Cu and Sn were initially adopted for the plasma diagnostic studies, which were used for verifying the functionalities of the Langmuir probe and the gridded energy analyzer (GEA). The two cathodes were arranged with an angle of 150 °, facing the substrate holder approximately 6 inches away. When using the ITO targets which are 3 inches in diameter, a pair of 3-inch magnetron (Circular Sputtering Source TORUS® 3″ HV, Kurt J. Lesker Co.) was used. The two magnetrons were installed in a similar pattern, with adjustable included angle and intruded depth into the chamber. Unless specially specified, the angle was set at 160 ° for most of the following experiments, and the distance between the magnetron surface and the substrate was approximately 3 inches. The side surface of each cathode was shielded by a stainless steel dark space shielding. The shortest distance between the two cathodes was about 1 inch. Such a magnetron geometry set a limitation for the secondary RF coil design. The dual magnetrons were driven by two separate dc power supplies. In this study, the power supplies were always operated in a constant-current mode, in a range of 0 to 100 mA per cathode.

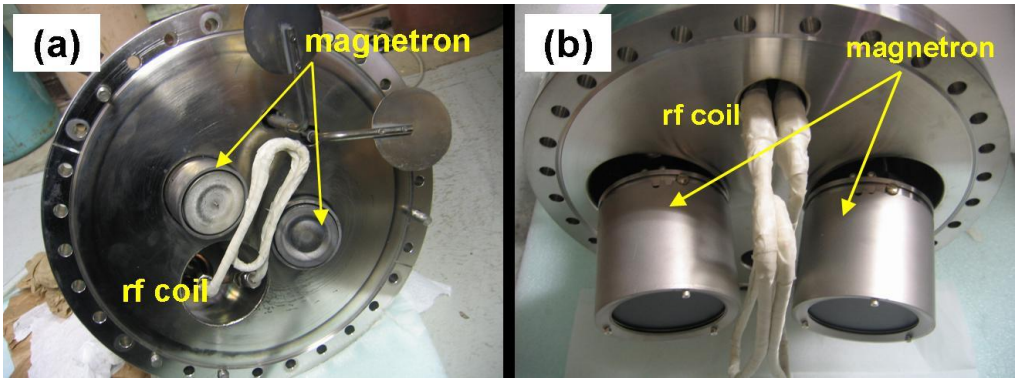

Figure 2.3 (a) The RF-assisted 2-inch magnetron with Sn targets. (b) The RF-assisted 3-inch magnetron with ITO targets.

One of our tasks was to study the RF enhancement of the plasma and consequently the ITO film deposition. The auxiliary RF coil installed in each magnetron can be seen in Figure 2.3. The coils were made of ¼ inch stainless steel tube. The two ends of the coil were connected to the water cooling and RF power outside through an RF feedthrough flange. Due to the geometrical restrictions, the design and the placement of the coil were not exactly the same in the 2-inch and 3-inch magnetron systems. The 2-inch magnetron system used a two-turn, 4.5 inches by 1.5 inches rectangle coil. It was bent inward slightly at the middle length to fit in between the two cathodes. The coil was in the same plane of target surface (roughly, since the magnetron has been inclined at a small angle), and was parallel to the substrate. The coil was wrapped with the fiber glass tape for a better insulation, considering it was close to the cathode. For the 3-inch magnetron system, a 2-turn RF coil was mounted perpendicular to the target surface to avoid contacting the dark space shielding. It was also larger, about 2 inches in width and 6 inches in length.

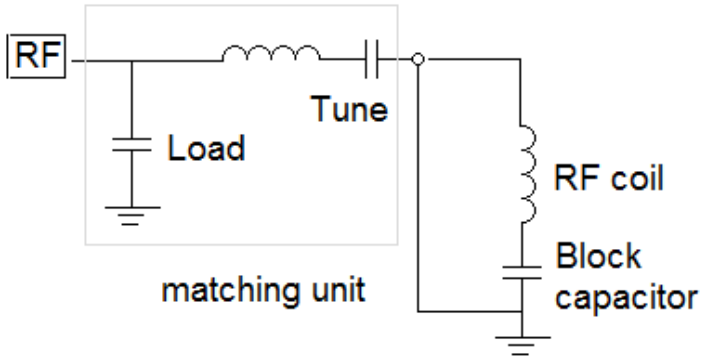

Figure 2.4 Electrical circuit diagram of electrical setup for RF system.

Figure 2.4 shows the schematic electrical circuit diagram of the RF system. A matching unit was hooked up to the output of the RF generator in order to reduce the RF power reflection. A blocking capacitor of 250 pF (voltage rated up to 15 kV) was placed between the RF coil and the "ground", which improved matching and reduced the self-bias generated on the coil [42]. It should be noted that the RF generators and the matching units used for 2-inch and 3-inch magnetrons were different. For the 2-inch magnetron, an RFPP 13.56 MHz RF-30 generator and a lab-made matching network were used. For 3-inch

magnetron, a package including a KJLC R601 600W power supply and an auto-match unit was used. With the auto-match unit, it was easier to maintain a stable plasma environment to carry out the experiments. The two different power generators are shown in Figure 2.5.

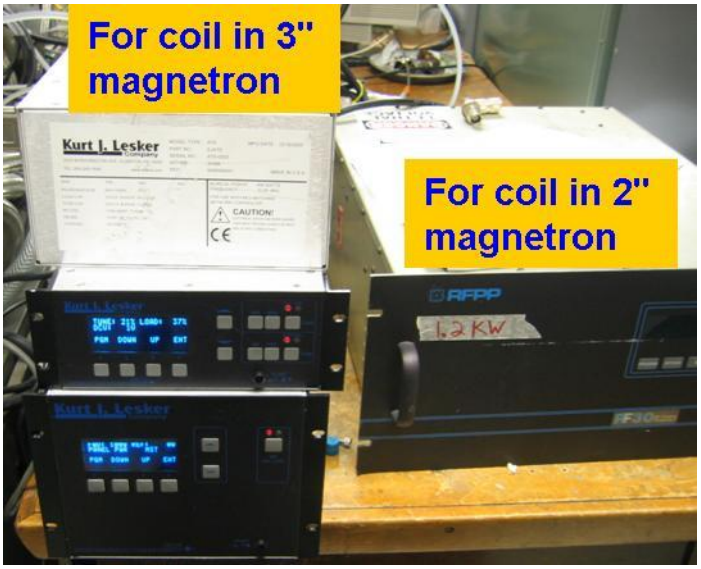

Figure 2.5 The RF generator and matching network for the RF coil, (left) for the coil in the 3-inch magnetron, (right) for the coil in the 2-inch magnetron.

2.1.2 Magnetron configuration

As mentioned in Chapter 1, the dual magnetron pair can be arranged in different configurations. The 2-inch magnetrons are "balanced" individually and were installed with the same polarity. This configuration was only used for the plasma diagnostic tests. Two identical magnetrons were run as balanced and coupled together with the same polarity setup, as illustrated in Figure 2.6 (left). The magnetic field strength of all the magnets is set such that the field lines all remain in closed loops, running from the inner magnet to the outer ones, and vice versa. Ideally, no magnetic field line connects to a magnet in the other magnetron. Meanwhile, the 3-inch magnetrons have a flexibility to alter the magnets arrangement inside. By reducing the strength of inner magnets, each 3-inch magnetron became unbalanced. By

reversing all the magnet polarities in one magnetron, some field lines connect the two magnetrons and a closed-field configuration was produced. The two magnetrons are balanced as a group, as shown in Figure 2.6 (right). The plasma is expected to extend to the intervening region between the two magnetrons.

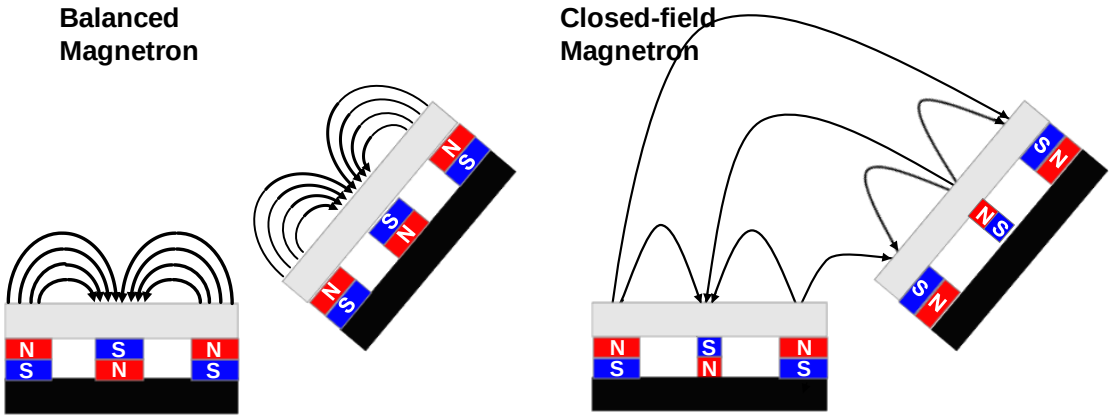

Figure 2.6 Two different configurations for the 3-inch dual magnetron. (Left) balanced mirrored configuration, (right) unbalanced closed-field configuration.

In an Ar ambient gas, a distinctive shape of the magnetron plasma was generated in the unbalanced closed-field configuration as compared with that of the balanced configuration. The plasma in the closed-field magnetron connects through the intervening area, extending to the substrate zone, as shown in Figure 2.7 (b).

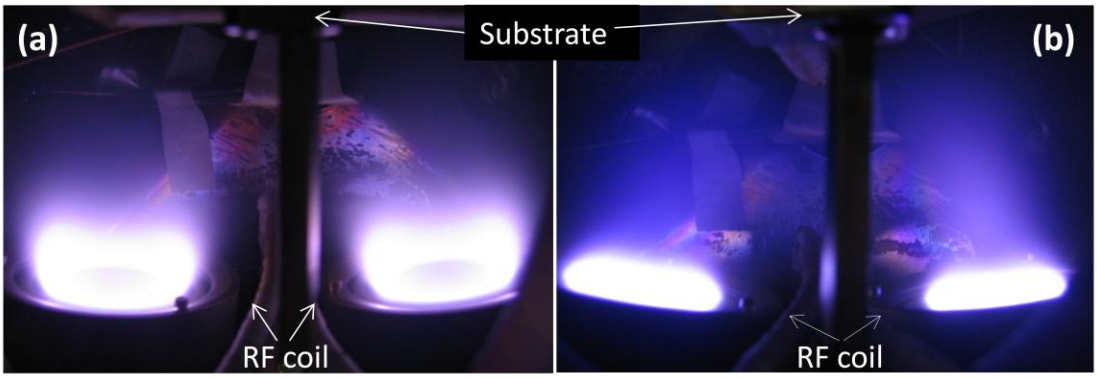

Figure 2.7 Cathode configurations: (*a*) balanced cathode configuration showing distinct ionization populations clustered at the magnetrons; (*b*) unbalanced closed-field configuration where the coupling of the magnetic field leads to electron sharing and glow in an arch through the intended substrate deposition zone.

2.2 Langmuir Probe

2.2.1 RF-compensated Langmuir Probe

A Langmuir probe is the simplest and most commonly used tool to determine the principal parameters of a plasma such as the electron temperature, electron density, and plasma potential. It works by inserting one or more electrodes into a plasma, with a constant or time-varying electric potential on the electrodes. For this study, a single Langmuir probe was used, which consists of only one probe tip. By changing the voltage on the probe and measuring the current collected, an I-V trace can be acquired, from which important plasma parameters can be derived. [43]

Figure 2.8 shows a constructed single Langmuir probe (RF-compensated). The material that the probe holder is made out of is not of a great concern to the probe operation as long as the signal is isolated and the material does not adversely affect or react with the plasma or vacuum conditions. In this case, an alumina tube and Torr Seal® were used, to minimize any outgassing into the vacuum chamber. A Kapton® coaxial cable with a grounded shield was used. At the end of the tube, the cable was stripped and a piece of tungsten wire was soldered to the center conductor, serving as the probe tip. The outer conductor of the cable served as a shield for noises, which is critical in an RF plasma. The tungsten wire probe tip has a diameter of 0.254 mm (0.01 inch), and a length of 3.60 mm. The probe tubing at the tip end is 3/16 inch in diameter and the whole probe is 6 inches long.

In an RF plasma, the effect of an oscillating plasma potential makes it difficult to take and interpret probe data. In Maxwellian plasmas, an average electron current can still give the correct electron temperature. However, RF interference varies the electron current taken out of the exponential region, and as a result an overestimation of electron temperature can occur. As such, RF-compensation for the probe is of the utmost importance. A constructed RF-compensated probe and its schematic diagram are shown in Figure 2.8.

Sudit and Chen found that the uncompensated probes yielded electron temperature measurements artificially higher by as much as 2 to 3eV. Because of the RF power source, there is a local fluctuation in the plasma potential in the area where the probe measurement is taken. This is corrected through the use of a compensation electrode. The electrode is placed near the probe tip and then coupled across a capacitor of 1 nF to the probe tip so that the tip may also follow the fluctuation in the plasma potential. The most critical aspect is getting the notch filters as close to the probe tip as possible so as to avoid the buildup of stray capacitance. [44]

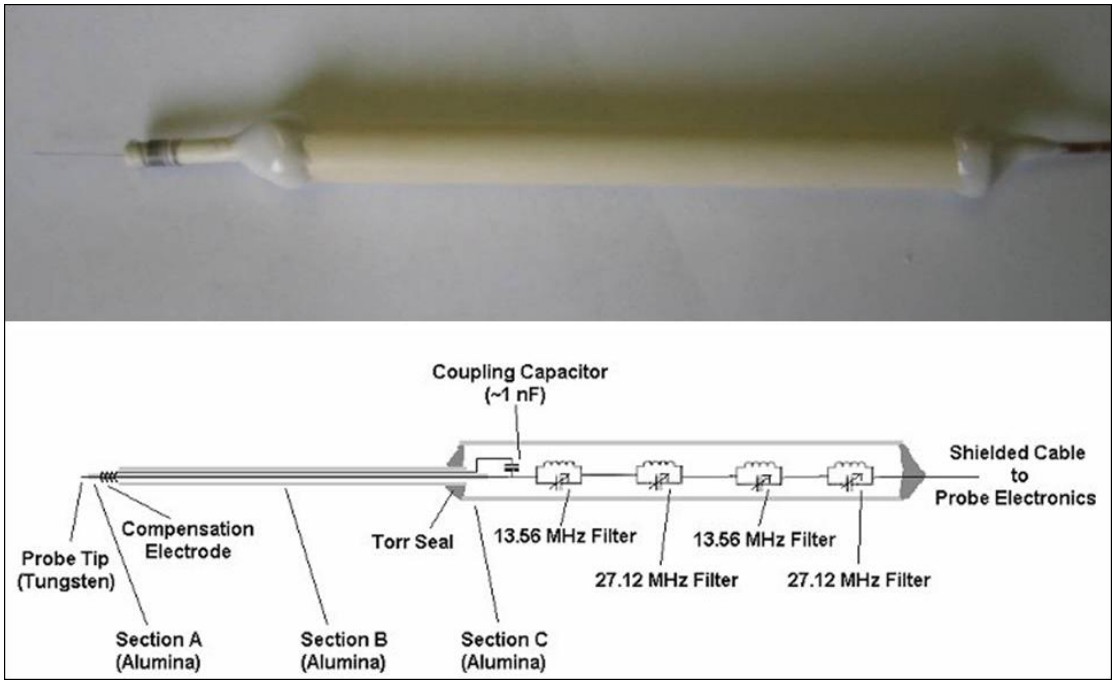

Figure 2.8. The RF compensated Langmuir probe employed in SHADE chamber. (a) A picture of actual probe. (b) Schematic diagram.

This RF compensated Langmuir probe has a series of built-in notch filters that have been tuned to block the 13.56 MHz and 27.12 MHz RF signal [45], while allowing the remaining frequency spectrum to pass through undamped. These filters consist of an inductor and capacitor in parallel. The inductance L and the conductance C were chosen to let the resonance frequency equal to 13.56 MHz or 27.12 MHz, so that the RF signals are blocked [46,47]. Specifically, inductors of 3.3 μH and 1.0 μH were used for the 13.56 MHz filter and

27.12 MHz filter respectively. Tunable capacitors in the range of 8-80 pF were used and tuned to filter the 13.56 MHz or 27.12 MHz signals. Two filters for each frequency are used in series so as to provide a greater amount of impedance.

2.2.2 Electrical setup for the Langmuir probe

The probe electronics are shown schematically in Figure 2.9. The Langmuir probe was connected to an electrical feedthrough. The probe signal went through a BNC cable to the oscilloscope. An RF filter with a similar design to that of the filters inside the probe was used at the oscilloscope input. It blocked most of the RF noise picked up in the BNC cable between the oscilloscope and the feedthrough. Additionally, by properly shielding the RF power supply, the matching unit and the joint to the RF power feedthrough, the RF noise pick-up was sufficiently suppressed.

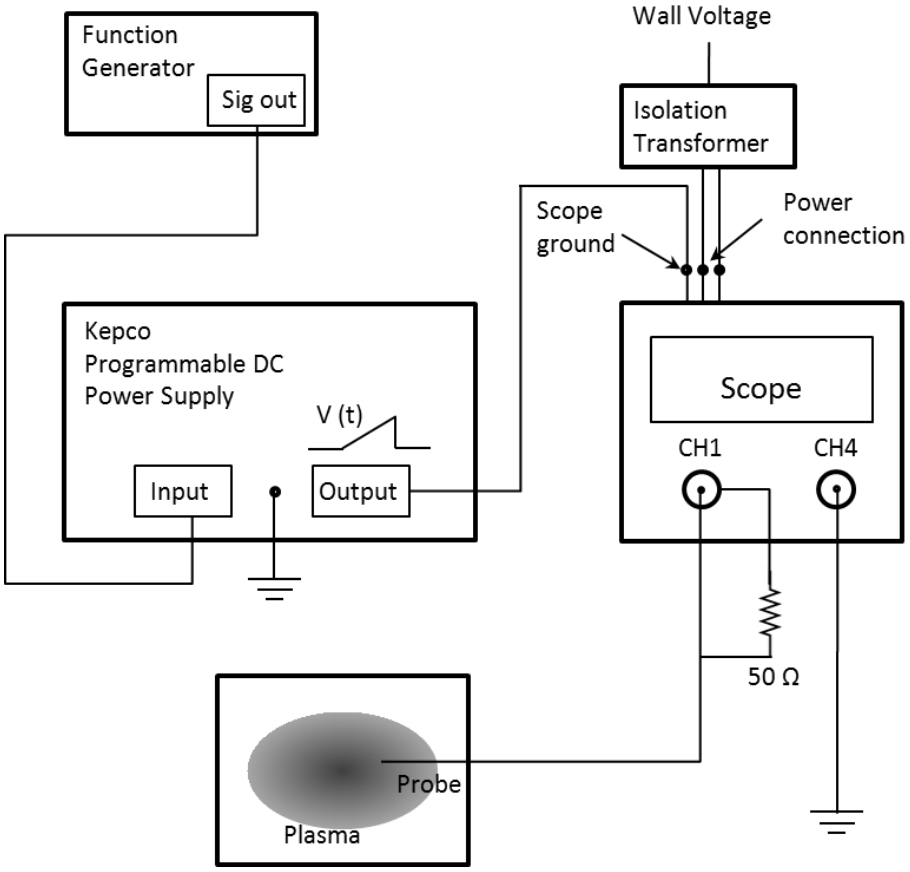

Figure 2.9 Langmuir probe circuit diagram

The probe driving circuit consists of a BK PRECISION 4011A 5 MHz Function Generator, a Kepco Bipolar Operational Power Supply/Amplifier (Model BOP 500M), a Tektronix TDS 2014 4-Channel Digital Storage Oscilloscope, and an isolation transformer to "float" the scope. The function generator created a continuous sawtooth waveform. The frequency, output level and the ramp time were set as desired. The voltage output from the function generator went to the input of a Kepco model BOP 500M bipolar amplifier ($\pm$ 500 V, $\pm$ 80 mA max), which amplified the signal by a factor of 100 and added an adjustable DC offset to it. The generated sweeping voltage (usually set between -40 and +40 volts) drove the probe.

The oscilloscope was intentionally isolated from the common/wall ground by using an isolation transformer between the oscilloscope and the wall outlet, as illustrated in Figure 2.9. This significantly reduced the noise pick-up from wall voltage. The scope ground was connected to the output of the Kepco amplifier as a "floating ground", rather than being connected to the common ground. The outer conductors of all the BNC connectors for different oscilloscope channels were at this varying voltage. The coaxial cable from the probe was attached to channel 1 via a T-connection BNC connector, and a 50 Ohm terminator was connected. This is equivalent to a connection of the center conductor (which goes to the probe) and the scope "floating ground" through a 50-ohm resistor. Thus that the channel 1 measured the voltage across the 50 ohm resistor, and the current collected by the probe could be easily calculated. In fact, this current was relatively small that the probe nearly followed the sweeping scope voltage, differing by a few volts at most. Meanwhile, scope channel 4 measured the voltage between the true ground and the oscilloscope's floating voltage (sweeping voltage output). During the probe data acquisition, both the probe current(s) and the sweeping voltage were measured by the scope. I-V traces were collected for multiple times (e.g. 128 times) and averaged in order to reduce noise.

2.2.3 3-dimension Langmuir probe diagnostics

It is of great interest to characterize the plasma at various conditions, so that the effect of the magnetron power, secondary RF power, pressure, and magnetron configuration on the plasma can be better understood. With a movable probe, a 3-D mapping of the plasma parameters can be obtained. This is quite beneficial for studying a large area deposition system. For example, the uniformity of the film deposition can be estimated by measuring the plasma spatial distribution.

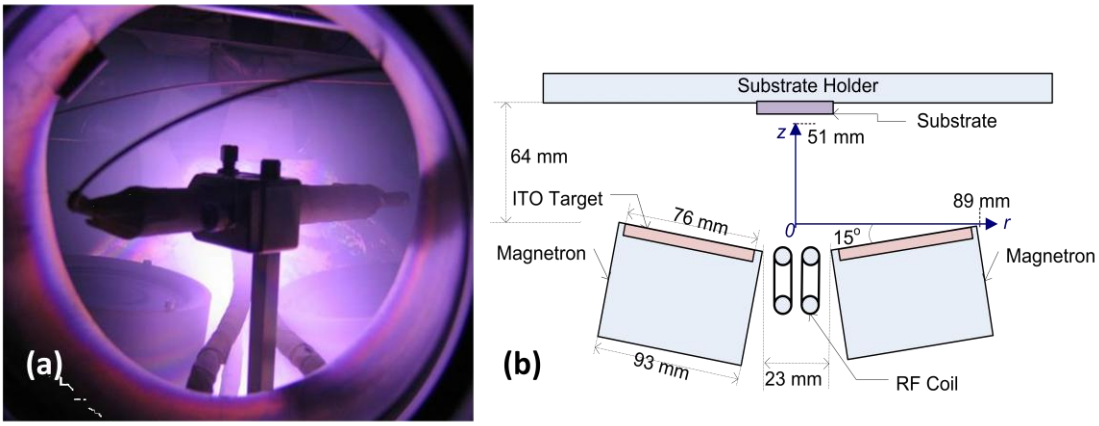

Figure 2.10 (a) 3-D scanning RF compensated Langmuir probe in SHADE chamber. (b) Spatial coverage of the probe (51 mm or 2 in. in z direction and around 89 mm or 3.5 inch in r direction).

The entire probe was mounted to a rotary-linear motion feedthrough such that it could be moved within a three-dimension region between the magnetron and the substrate (Figure 2.10 (a)). The probe tip could scan linearly from the magnetron surface to the substrate and laterally from the midpoint of the two magnetrons to the farther end, i.e., 51 mm (2 inch) in *z* direction (z=0 corresponding to the outer edge of the magnetron) and 89 mm (3.5 inch) in *r* direction, as shown in Figure 2.10 (b). The performances of the unbalanced closed-field magnetron and the balanced magnetron were compared using this scanning Langmuir probe. The magnetrons were run at 50 mA of current in 5 mTorr Ar without RF assistance. The influence of the coupled RF plasma on the Ar sputtering plasma was subsequently investigated. Using a closed-field magnetron configuration and the same settings of

magnetron current and pressure as above, the RF power was increased from 0 to 200 W when the spatial distribution of electron density n_e and temperature T_e were measured. It should be noted that a decrease of the voltage on the DC magnetron approximately from 230V to 170V was observed as the RF power was increased. The analysis and discussion of these Langmuir probe diagnostics are presented in Chapter 3.

2.3 Gridded Energy Analyzer

2.3.1 Concepts of gridded energy analyzer

In this RF-assisted closed-field magnetron, the ionization of sputtered atoms is expected to be enhanced, improving the ITO film properties. It is important to directly measure the ionization fraction under different conditions. There are different methods to estimate the ionization fraction. The computer simulation has been widely used for the plasma modeling [48-50], however, these models still have difficulty in predicting exactly the on-wafer plasma characteristics for a complicated iPVD system. The direct characterizations of ionization fraction by absorption spectroscopy and energy-resolved mass spectrometry have been developed [51-53]. But the absolute ion fraction from the spectral data has often been found to be inaccurate because of many unknown collisional cross-sections of low ionization states and a significant deviation of the electron energy distribution from the Maxwellian distribution [54]. A typical mass spectrometer, however, requires a substantial space for its differential pumping hardware which makes it difficult to be adapted into a production iPVD system.

A simple in-situ ion fraction measurement can be realized by a gridded energy analyzer (GEA) combined with a quartz crystal microbalance (QCM) [55-57]. Rossnagel et al introduced the QCM in the inductively coupled RF plasma to measure the deposition rate of metal fluxes and thus the metal ionization fraction [55]. However, their design was only useful at low plasma densities. Higher density plasma will penetrate the grids due to a much thinner sheath around the mesh wires. Bohm addressed issues regarding the GEA design particularly with respect to the choice of grid material and dimensions [58]. Green et al built a similar instrument and improved its performance by employing a three-grid GEA to reduce plasma penetration and biasing the QCM at the potential of the substrate. The shadowing effect of non-directional neutral flux by the GEA casing wall should be considered for the calibration of the ionization fraction [56].

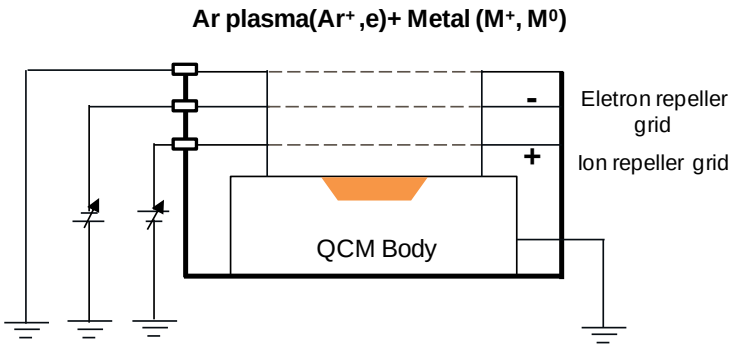

Figure 2.11 Schematic diagram of the GEA and QCM assembly.

Figure 2.11 shows the schematic diagram of the GEA located above the QCM. The top mesh grid was grounded to minimize the disturbance to the plasma while the middle grid (the electron repeller grid) was negatively biased around -15V to further reduce the electron penetration. The bottom grid, which acted as the ion repeller, was applied with an adjustable potential of -10V to 50V. The total fluxes of metal ions and neutrals Φ_{tot_QCM} admitted to the QCM sensor could be determined when the ion repeller grid was negatively biased. When a positive bias was applied to the grid and gradually increased up to 50V, only the neutral flux Φ_{N_QCM} reached the QCM [59]. The ion flux Φ_{ion_QCM} received by the QCM was obtained by subtracting the neutral flux from the total flux as Equ. 2.1. To calculate the actual ion flux Φ_{ion_plasma} and neutral flux Φ_{N_plasma} before entering the GEA, the transparency T_g due to each grid should be taken into account as given in Equ. 2.2 and 2.3. Moreover, for the non-directional neutral flux, the GEA casing shadowed an extra fraction of the flux from reaching the QCM sensor, inducing a geometrical factor *G*. A more specific description of the calculation of G was done by Green *et al* [56]. For normally incident ions governed by electric field, the ion fluxes at the QCM sensor and those at the substrate are the same if there are no screens present and the factor G is simply unity as implied in Equ. 2.3. Φ_{ion_plasma} and Φ_{N_plasma} were further used to determine the ionization fraction (*IF*) of the metal flux as given in Equ 4.2.

$$\Phi_{ion\_QCM} = \Phi_{tot\_QCM} - \Phi_{N\_QCM} \quad 2.1$$

$$\Phi_{N\_QCM} = \Phi_{N\_plasma}(G)(T_g)^3 \quad 2.2$$

$$\Phi_{ion\_QCM} = \Phi_{ion\_plasma}(T_g)^3 \quad (2.3)$$

$$IF = \frac{\Phi_{ion\_plasma}}{\Phi_{ion\_plasma} + \Phi_{N\_plasma}} = \frac{\Phi_{tot\_QCM} - \Phi_{N\_QCM}}{\Phi_{tot\_QCM} - \Phi_{N\_QCM} + \Phi_{N\_QCM}/G} \quad (2.4)$$

The individual effects of input power and pressure on the ionization efficiency were investigated. Since the GEA and QCM assembly was mounted on a rotary-linear manipulator, the ionization fraction could be measured at different locations.

2.3.2 Ionization Measurement by GEA/QCM

Figure 2.12 (a) shows a constructed GEA. The three layers of grids are made of stainless steel mesh (60×60 wires per inch, 0.0045 inch wire diameter, percentage of open area 53.3%). The total transparency of grids is about 15%. The GEA consists of a top cover of thin stainless steel but with an opening at the center as the inlet for deposition flux. The top grid is welded to this cover and electrically grounded. All the grids are insulated to each other by Teflon® disks, glued together by Torr Seal® and finally encapsulated by a turn of stainless steel shim, also grounded. Each of the middle and bottom grids is soldered to the center conductor of a Kapton® coaxial cable, for the purpose of independent biasing. The other end of the cable is the BNC connector so as to hook up easily to the biasing power supply through an electrical feedthrough flange. The inner diameter of opening of the GEA is about 0.80 inch and total height of the GEA is 0.41 inch. For the metal flux measurement, the GEA was put above an Inficon Front Load Dual Sensor QCM, with its center opening aligned with one QCM crystal, as shown in Figure 2.12 (b). The QCM was water cooled and the second sensor could be used to monitor the flux change due to the varying temperature. The whole assembly was in the same plane as is the sample holder, and was approximately 3 inch below the holder. Unfortunately, the position could not be adjusted with the QCM being fixed. An Inficon XTC/2 Thin Film Deposition Controller outside the chamber was used to read the QCM signals, i.e., the deposition rate or mass change rate on the crystal sensor.

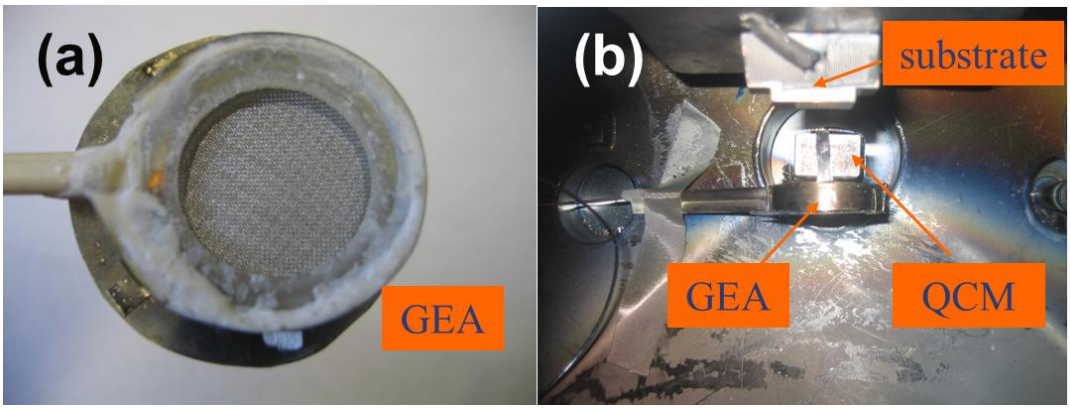

Figure 2.12 (a) Picture of a gridded energy analyzer with Teflon® disks to insulate the screens. Total transparency of the three layers of grids is 15%. (b) GEA and QCM measurement setup in the chamber, located right below the substrate sample holder.

The ionization fraction measurements were performed in both the balanced and unbalanced closed-field magnetron configurations and compared with each other. The effect of the RF power on the ITO ionization fraction was studied by varying the RF power from 0 to 400W, while the magnetron cathode current and the gas pressure were fixed (50 mA and 5 mTorr/0.67 Pa, respectively). Then without any RF assistance, the pressure was adjusted from 1 to 20 mTorr (0.13-2.67 Pa) to measure the variation of the ionization fraction. The data and discussions are presented in Chapter 4.

2.4 ITO Film Depositions

2.4.1 Film Deposition

The ITO film was deposited in the prototype RF-assisted closed-field magnetron system. Both glass and Polyethylene Terephthalate (PET) were used as substrates. As shown in Figure 2.13, a glass slide was attached to the sample holder using some double-side carbon tape. A piece of PET sheet (0.005 inch thick) was cut slightly longer than the width of the sample holder. By taping it at both ends, the PET substrate was bent upwards. Since it didn't touch the sample holder, no cooling was applied to the PET substrate. A temperature indicator was placed at the back side of the PET to record the substrate temperature during the deposition. A piece of Kapton tape was used to cover a small area of glass and PET, so that the profilometry could be performed afterwards. After the sample holder was transferred into the chamber via loadlock, Ar and O_2 gas combinations were introduced inside under the control of mass flow controllers. The chamber pressure during the deposition was kept at 5 mTorr (0.67 Pa) and the amount of O_2 in the gas mixture was at about 2% in volume. The DC magnetron current was set at 90 mA per cathode, while the RF Power was varied between 0 and 400 W. Under these conditions, the ITO films were deposited for up to 45 min and no extra annealing was carried out which could further modify the ITO film properties. Various characterizations of the films were performed to determine the thickness, sheet resistance, transmittance as well as the composition and micro-structures.

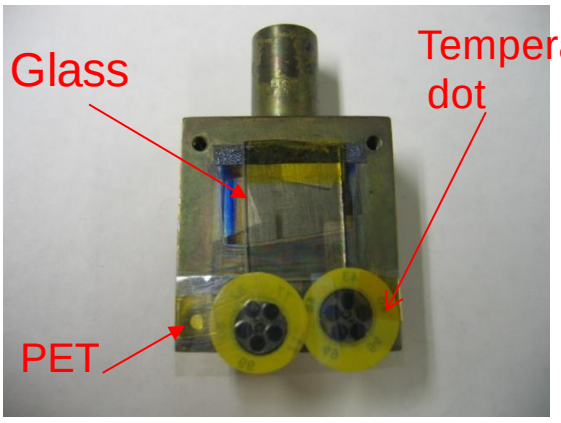

Figure 2.13 Glass and PET substrates arranged on the sample holder.

After the film depositions in the small scale 3-inch (76-mm) magnetron system, the prototype system was adapted for a large area roll-to-roll deposition system with dual 3.5×18 inch rectangular magnetron cathodes, as shown in Figure 2.14. Because the magnetic design of the larger cathode was very difficult to modify, the stock balanced configuration was utilized for both cathodes, with the exception of reversed polarity on the second device. The two linear cathodes were mounted at a 90 °included angle (Figure 2.14, left). An RF coil was modified and fabricated to fit in this larger scale system as the RF plasma source (Figure 2.14, right). It was made out of ¼ inch stainless steel tubing, and was in a rectangular shape of 18 inches long and 3 inches wide. A rotation stage was affixed with posts to form a four-sided 7-inch wide structure on which to attach the PET substrates. The rotation stage was utilized as a shutter mechanism to rotate the substrates into the deposition zone and start the deposition. Deposition timing repeatability is on an order of 1 second. All cathode operations were performed in a DC constant current mode. A magnetron current of 810 mA was initially chosen to achieve the same current density as in the 3-inch magnetron system, and was further increased up to 1600 mA per cathode. The O_2 partial pressure could be maintained at a low level of < 1%. The effect of RF power on the ITO deposition was also studied in this large area linear cathode system.

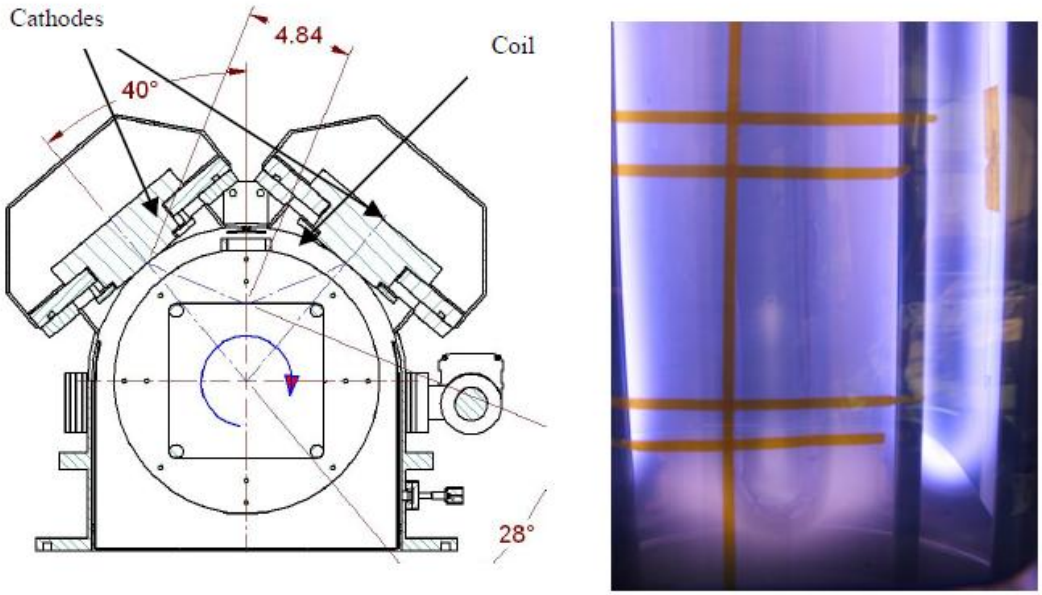

Figure 2.14 Deposition system geometry (left); The two cathodes and the coil in operation during the deposition, viewing through the clear substrates and supporting PET web. Kapton tape was visible in the image holding the substrate in place (right).

2.4.2 Characterization techniques

To determine the film qualities of ITO, the foremost conductivity (resistivity) and the transmittance of light were first measured. The former was performed using a four-point probe system and a surface profilometer. The four point probe measures the sheet resistance Rs, as a measure of resistance of thin films that have a uniform thickness. Sheet resistance is applicable to two-dimensional systems where the thin film is considered to be a two-dimensional entity. It is analogous to resistivity as used in three-dimensional systems. The bulk resistivity ρ could be calculated as

$$\rho = R_s * t \qquad 2.5$$

where t is the film thickness. The units of sheet resistance are ohms. An alternate, common unit is "ohm per square" (denoted as "Ω/sq"), which is dimensionally equal to an ohm, but is exclusively used for sheet resistance. Using an X-Rite 361T optical densitometer, the average light transmittance of the ITO film in the visible spectrum (340-650 nm) was determined from the measured optical density, after corrected for the contributions of the uncoated substrate.

Other than the film conductivity (resistivity) and the transmittance, other surface analysis techniques were also employed to explore different factors affecting the film qualities. X-ray photoelectron spectroscopy (XPS) was used to measure the composition of the films and determine the stoichiometry of the obtained ITO. Since the surface microstructure may affect the film properties, atomic force microscopy (AFM) was used to study the film surface morphology and its potential interrelationship with the film properties.

Chapter 3 Langmuir Probe Diagnostics

In this chapter, the diagnostics of the plasma using an RF-compensated Langmuir probe are presented. A typical method was used to analyze the probe I-V traces and find the electron density and temperature of the plasma. Such diagnostics were very handy to reveal the influence of individual parameters on the plasma, and further help optimize the processing. A 3-D scanning Langmuir probe was first tested in the 2-inch balanced magnetron using Sn targets. A more detailed investigation was performed in the 3-inch magnetron with ITO targets. The 3-inch magnetron was operated in either balanced or unbalanced closed-field configuration. Under a same DC magnetron current, a denser and more diffusive plasma was observed in the closed-field magnetron, which could benefit the film deposition. The influence of the coupled RF power on the sputtering was investigated. An increase of the RF power from 0 to 200 W enhanced the plasma density by one or two orders of magnitude.

3.1 Data Analysis Method

The method for analyzing the Langmuir probe traces used for in this thesis is based on Ref. [43]. The basic steps of the method are concluded below.

a) Determine the floating potential V_f and the plasma potential V_p. V_f could be easily found to give zero probe current. V_p is determined to have the lowest dI/dV value (as the "knee" point of the trace).

b) Determine the length scale regime. There are three length scales to compare, the probe radius r_p, the electron neutral mean-free-path λ_0 and the Debye length λ_D. The first one is directly measured, while λ_0 depends on pressure. The Debye length λ_D is a function of T_e and n_e, which are exactly what we wish to find. Fortunately, T_e could be estimated by

$$V_p - V_f = T_e(3.34 + 0.5\ln(\mu)) \tag{3.1}$$

where plasma potential V_p and floating potential V_f could be found from raw data, and μ is the multiples of the hydrogen atom mass. Meanwhile, n_e could be estimated from the saturated

electron current at V_p. With these estimated T_e and n_e values (though they are not very accurate), the Debye length could be obtained. Then by comparing these three parameters, the sheath could be determined as thin or thick, collisionless or collisional. In our experiments, the sheath was always collisionless, but depending on electron density, it could be thin, thick or intermediate sheath.

c) Ion current subtraction and electron density determination. The ion current at a given probe bias V, according to a simplified model, is proportional to square root of V_p-V. Therefore, the ion saturation region of the raw data can be fit to be a parabola that has its apex at V_p and opens towards the y-axis. A point needs to be picked in the ion saturation region to do the fitting. The electron density could then be found from the ion saturation current I_i,

$$I_i = \frac{1}{4} e n_e \sqrt{\frac{8e}{\pi m_i}} A_p (1.127) \sqrt{V_p - V} \tag{3.2}$$

where A_p is probe collecting area. This calculated ion current is then subtracted from the total probe current to give only the electron current.

d) Determination of electron temperature. It could be found based on

$$\ln(|I_e(V)|) = \frac{-e}{kT_e}\left(V_p - V\right) + \ln\left(|I_{esat}|\right) \tag{3.3}$$

So by plotting the natural log of the electron current vs. (V_p-V), T_e could be obtained as the reciprocal of the slope in units of eV.

e) If the sheath is not in the scope of a thin or thick sheath regime but transitional, the Laframboise method was used for the analysis. A unitless value j_i^* needs to be considered to get the effective collection area of the probe, accounting for the Bohm acceleration in the pre-sheath. It could be determined from a Laframboise plot as shown in Figure 3.1. With this constant, the correlation between n_e and ion current becomes

$$I_i = \frac{1}{4} e n_e \sqrt{\frac{8e}{\pi m_i}} A_p j_i^* \tag{3.4}$$

f) Error analysis. There are always various errors for the measurements of electron temperature and density. First of all, the errors could arise from the disturbance of the bulk plasma by the mere presence of the probe. This is an intrinsic drawback of the probe diagnostics as contrasted to a non-intrusive method such as optical emission spectroscopy. It's

difficult to quantitatively determine this kind of error, and thus in the present thesis it is not incorporated in the error analysis. Second, each acquired point of current and voltage has a certain error, which further leads to an uncertainty of the ion saturation current and thus electron density. In a typical measurement, the I-V traces are taken over a short period of time and get averaged for 128 times. In this way, this error could be reasonably suppressed. Finally, an error could be generated during the data analysis process. For example, due to a non-ideal I-V curve, the reciprocal of the slope of the electron current curve usually deviates from a straight line, causing an uncertainty in the determination of T_e and consequently n_e. In this thesis, the error bars were analyzed based on the last two causes. However it should be kept in mind that an additional error of about $\pm 20\%$ could originate from the plasma disturbance.

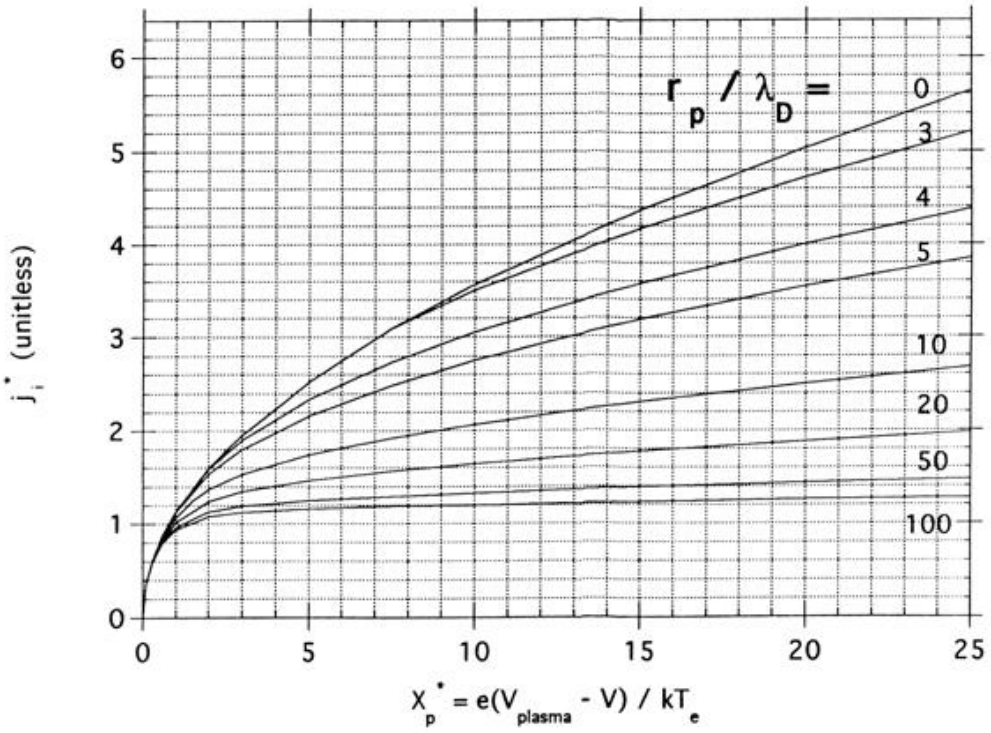

Figure 3.1 Laframboise plot [43]. The x-axis is a dimensionless parameter indicating how far the probe is biased into ion saturation compared to the electron temperature. j_i^* is the resulting dimensionless parameter that multiplies the geometric area of the probe to give the effective collection area for ions.

3.2 Probe Diagnostics in the 2-inch Magnetron

The RF-compensated probe was first tested in the 2-inch magnetron using the Sn targets. The purpose was to verify the functionality of the probe in an RF plasma, and to get a rough idea of the influence of different parameters, such as the RF power and pressure, on the plasma. The system was operated in three different modes: DC magnetron alone, RF plasma alone and the combination of them. The typical plasma generated for each case is shown in Figure 3.2.

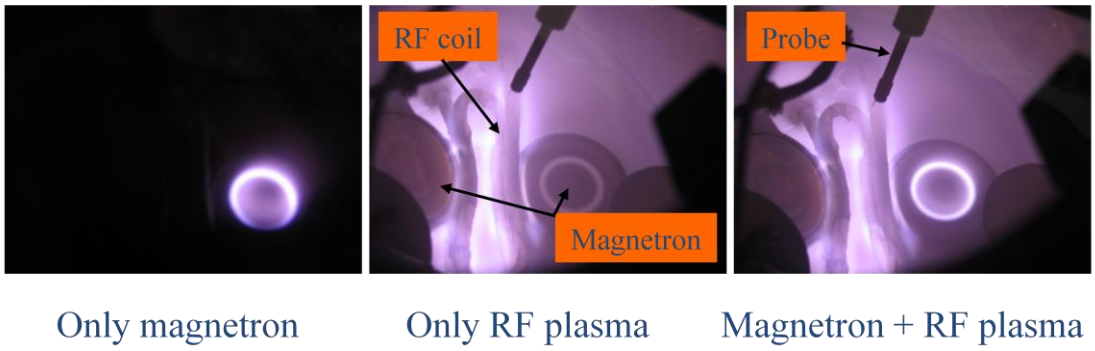

Figure 3.2 Plasmas in 2-inch magnetron with RF coil. Three different operation modes are compared.

First, the Langmuir probe measurements were performed in an RF plasma without initiating a DC magnetron discharge. The RF power was increased from 100 to 500 W. The Ar pressure in the chamber was kept at 10 mTorr by adjusting the flow rate. The probe tip was fixed at 2 inches in front of the RF coil. Figure 3.3 shows the dependence of the measured electron temperature T_e and density n_e on the RF power. T_e slightly decreased from 2.3 ($\pm$0.2) to 2.1 ($\pm$0.2) eV. Considering the error in measurements and analyses, T_e could be deemed as constant under different RF power inputs. Meanwhile, n_e significantly increased from 5.4×10^{9} ($\pm$ 8%) to 4.5×10^{10} ($\pm$ 8%) cm^{-3}. The increase of electron density was evidenced by the observance of a brighter plasma.

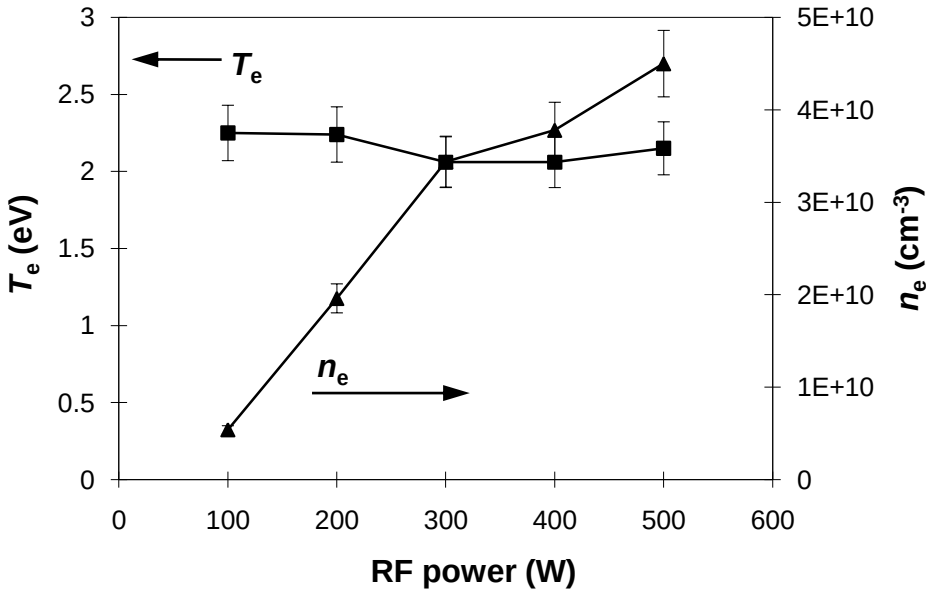

Figure 3.3 T_e and n_e of plasma at different RF power (10 mTorr, no magnetron discharge).

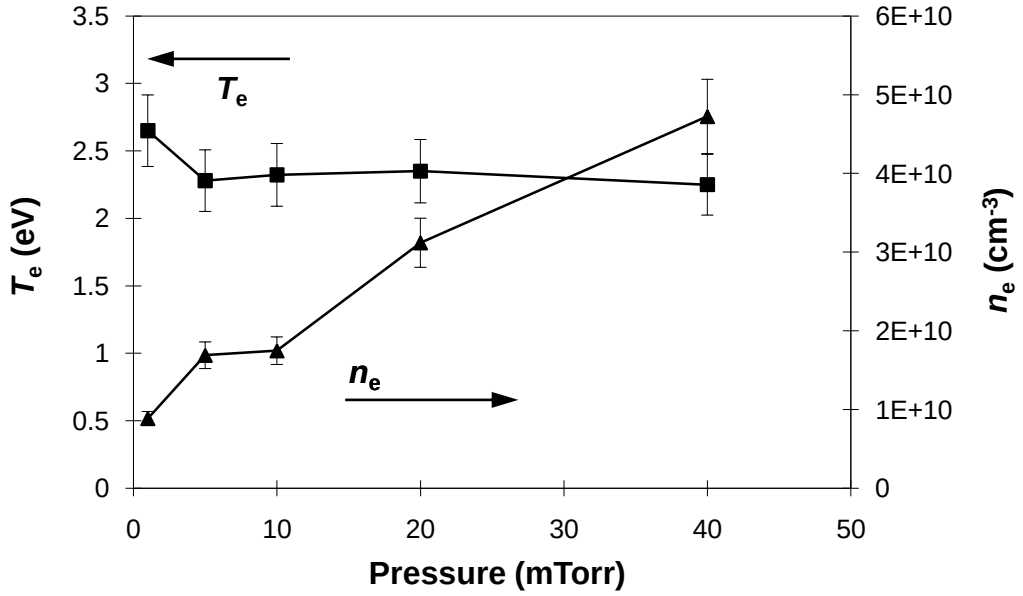

Figure 3.4 Effect of pressure on the RF plasma (250 W RF power, no magnetron discharge).

Next, the gas pressure was varied from 1 to 40 mTorr, with the RF power kept at 250 W. The probe was at the same position as in the previous test. As shown in Figure 3.4, n_e increased almost linearly with a higher pressure which should originate from an increased electron impact ionization frequency. T_e was measured to slightly decrease with pressure, from 2.7 ($\pm$0.3) to 2.3 ($\pm$0.2) eV. The higher T_e at the lower pressure is probably because of less electron scattering and as a result less energy loss.

For this RF-assisted dual magnetron system, it is desirable to study the magnetron performance under the RF assistance. The two cathodes were operated at a same current of 40 mA while RF power was varied from 0 to 400W. The probe was at the same position of 2 inches in front of the RF coil and the analyzed data are shown in Figure 3.5. The density of the magnetron plasma alone was as low as 1.4×10^{9} ($\pm$ 10%) cm^{-3}. It well reflects the observance in Figure 3.2, that the magnetron plasma had a bright racetrack but at the position where probe was located it was very weak. With an increasing RF power, n_e increased about linearly. With a 400W RF input, n_e reached 5.2×10^{10} ($\pm$ 10%) cm^{-3}, 37 times the density of DC magnetron plasma alone. T_e at different RF power was also calculated. Without RF assistance, it was measured to be as low as 0.7 eV (not shown in the plot), but the probe signal was too weak that the analysis was questionable. Usually, T_e for magnetron can be as high as about 8 eV [43]. Repeated measurements are necessary in the future to confirm the value. When the RF was applied, a trend could be seen in Figure 3.5. T_e of the DC magnetron+RF plasma decreased from 2.9 ($\pm$0.2) to 2.0 ($\pm$0.2) eV as the RF power was increased from 50 to 500W. Such a decrease of T_e with increased power has been commonly observed, likely because of the rapid energy loss of electrons due to the enhanced collisions [40]. In all, n_e was significantly increased and T_e was slightly decreased with the RF assistance, which could benefit a high-quality thin film deposition.

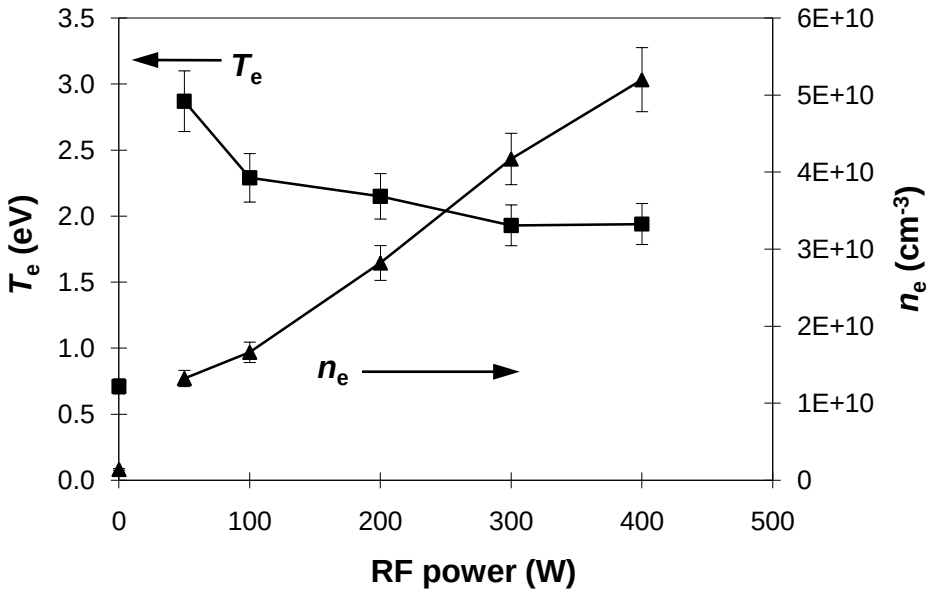

Figure 3.5 Plasma of the DC magnetron (40mA per cathode) with different RF assistance.

Subsequently, the effect of cathode current was studied. The current was increased from 0 to 80 mA, while 250W RF was always added to the system to avoid a too weak magnetron plasma. Measured T_e and n_e are plotted in Figure 3.6. Electron density scaled with an increasing cathode current, which makes sense since stronger and stronger magnetron plasmas were generated. T_e, however, did not change monotonically. Comparing with the RF plasma alone, applying the 5mA current to the magnetron increased T_e. As the current was further increased up to 80 mA, T_e decreased from 3.2 (± 0.3) to 2.2 (± 0.2) eV, which is similar to the increased RF power case shown in Figure 3.5. In contrast with an RF discharge, adding a magnetron discharge creates a high voltage sheath near the cathode, accelerating the electrons and increasing the overall electron temperature. Further increase of the magnetron discharge current leads to a higher plasma density and thus a greater chance for the electrons being scattered by the atoms or by ions (i.e. the Coulomb collisions), which lowers the average electron energy. Also as more metal atoms being sputtered out, electrons lose energy more easily since metal atoms have a lower ionization energy than Ar atoms.

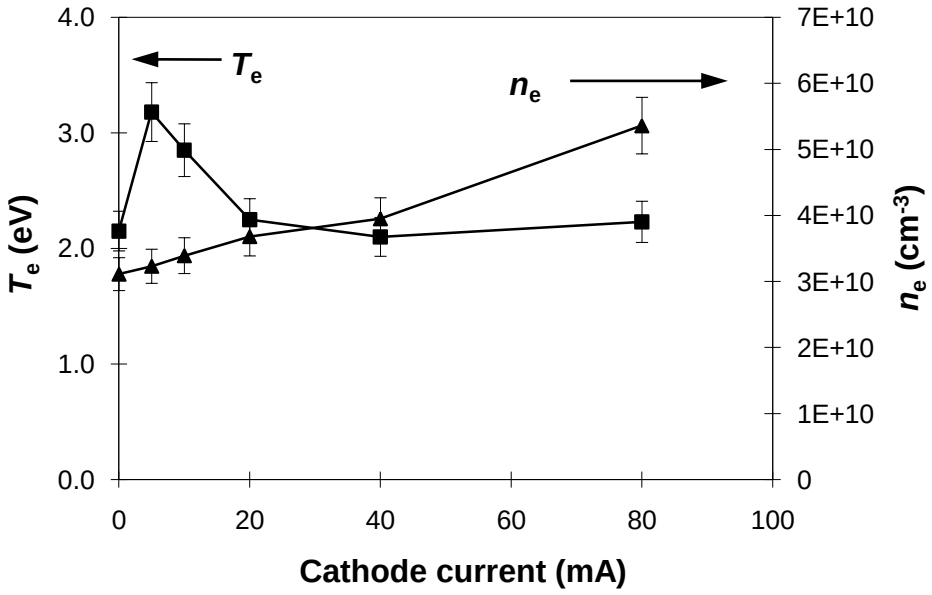

Figure 3.6 Effects of cathode current on the RF plasma (250 W RF power, no magnetron discharge).

The tests in the 2-inch magnetron showed that the constructed RF compensated probe worked in different operation modes. However, measuring a DC magnetron plasma of low cathode current without any RF assistance was difficult. Thus the plasma of RF enhanced magnetron was compared with magnetron plasma or RF plasma itself. The effect of secondary RF power, cathode current and other process parameters such as pressure were investigated. A significant increase of n_e by an increased RF power input was observed, as T_e was reduced accordingly. The electron density n_e scaled with a higher gas pressure while T_e did not change significantly with a possible slight decrease. Higher DC magnetron current also enhanced the plasma density. Subsequently, the probe was used for plasma diagnostics in the 3-inch magnetron pair with ITO targets.

3.3 Probe Diagnostics in the 3-inch Magnetron

In this section, the RF-compensated probe measurements performed in the 3-inch dual magnetron with ITO targets to study the plasma affected by various parameters are described. The magnetron pair was first set up in a balanced configuration. The influences of the RF assistance and ambient gas pressure were investigated. The probe was scanned in three dimensions to obtain the spatial distributions of T_e and n_e for both the DC magnetron plasma and the RF enhanced plasma. Then plasma diagnostics were performed in the closed-field unbalanced dual magnetron. The plasma properties in these two configurations are compared to study the effect of the magnetron configuration and to further understand the following experiments of metal ionization measurements and ITO film deposition.

3.3.1 Effect of the RF Power and Pressure

The diagnostics in the 2-inch balanced dual magnetron were presented in the previous section. After switching to the 3-inch magnetron, the balanced configuration was used to repeat those tests, i.e. the single variable tests (SVT) of RF power and the pressure. The configuration of the 3-inch dual magnetron was described in Section 2.1.

The RF power was varied from 50 to 400 W without initiating a magnetron discharge. The chamber pressure was 5 mTorr. The probe was placed 2 inches in front of the RF coil. It is denoted as z=2 inch and r=0. Here, z=0 corresponds to the outer edge of the magnetron, and r=0 corresponds to the midpoint of the two magnetrons. Figure 3.7 shows the effect of RF power on T_e and n_e. Similar trends as seen in the 2-inch magnetron were observed. T_e slightly decreased from 3.2 (± 0.3) to 2.8 (± 0.2) eV and basically kept constant with an RF power increased beyond 100 W. Meanwhile, n_e significantly increased from 4.8×10^{9} (± 10%) to 1.1×10^{12} (± 10%) cm^{-3}. A much higher electron density was obtained compared with the 2-inch magnetron case even with the same RF power applied. This shouldn't have been caused by a pressure difference since the pressure here was even lower (5 mTorr instead of 10 mTorr in 2-inch magnetron). The new coil design and the automatic matching unit should be

accounted for this difference. A larger fraction of the power was utilized for the plasma generation rather than being dumped on the blocking capacitor.

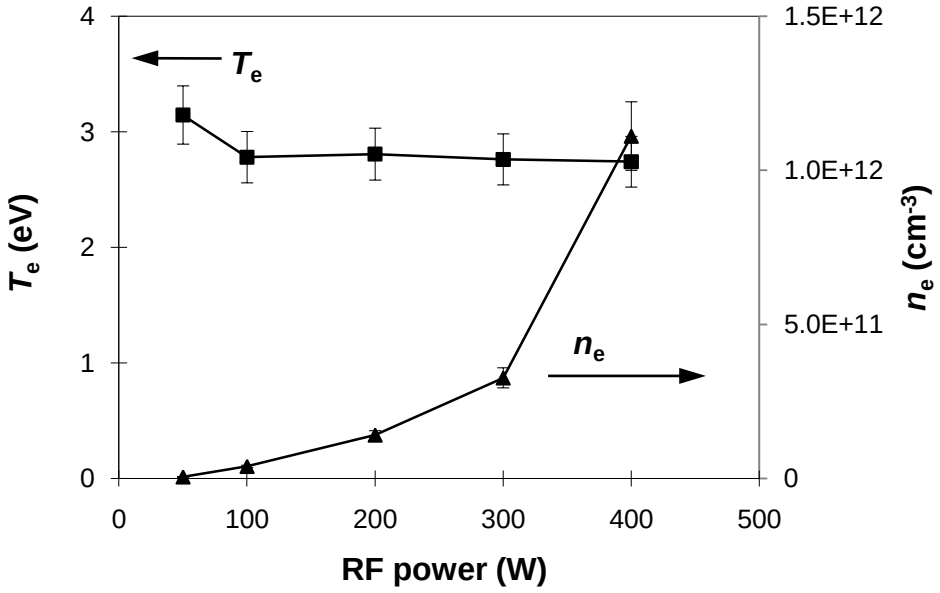

Figure 3.7 Effect of RF power on the plasma in 3-inch magnetron (5 mTorr, no magnetron discharge).

The gas pressure was then varied from 1 to 20 mTorr, while the RF power was fixed at 200 W. The probe was at the same position as in the RF power SVT test. Again, similar trends were observed as in the 2-inch magnetron, as shown in Figure 3.8. T_e was measured to decrease with pressure, from 3.0 ($\pm$0.2) to 2.4 ($\pm$0.2) eV, and n_e generally increased with the pressure. A higher pressure leads to a reduced mean free path for electron collisions, so that electrons ionize the atoms more frequently to give a higher plasma density, during which electrons easily lose their energy resulting in a reduced electron temperature. At around 10 mTorr, n_e reached a maximum point. It is likely at a higher pressure than 10 mTorr, the greatly decreased electron temperature significantly reduces the ionization efficiency.

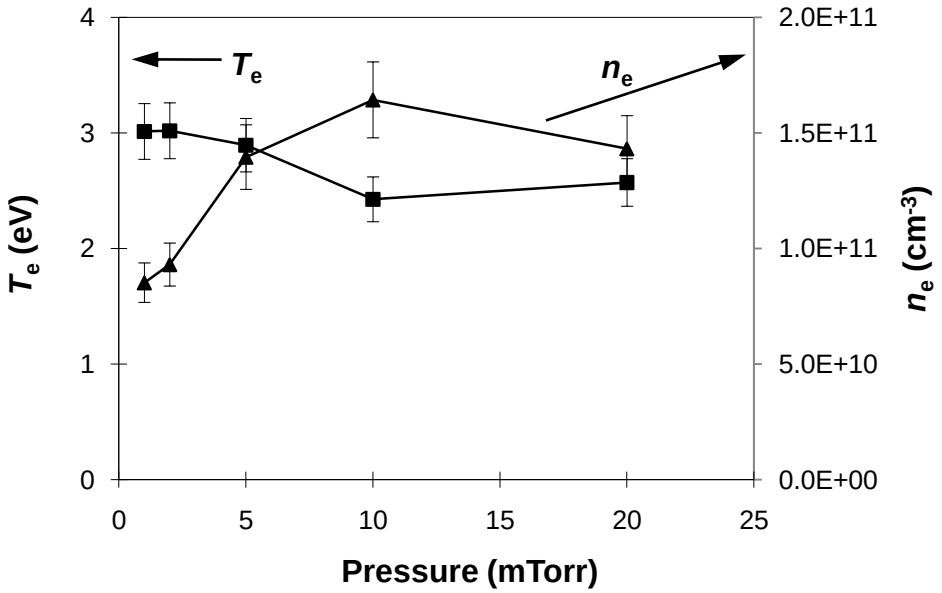

Figure 3.8 Effects of pressure on plasma in the 3-inch magnetron (200W RF, no magnetron discharge).

3.3.2 Effect of the Magnetron Configuration

The performances of the closed-field magnetron and the balanced magnetron configuration were compared using the 3-D scanning Langmuir probe. The probe tip was moved linearly from the magnetron surface to the substrate and scanned laterally from the midpoint of the two magnetrons to the farther end, 51 mm in the z direction (z = 0 corresponding to the outer edge of the magnetron) and 89 mm in the r direction (r = 0 corresponding to the midpoint of the two magnetrons), as shown in Figure 2.10. It should be noted that for all the 3-D measurements, a millimeter (mm) has been used as the unit. The magnetrons were run at a magnetron current of 50 mA per cathode and in 5 mTorr of Ar, for both the balanced and closed-field unbalanced configurations.

In order to highlight the differences of magnetron plasmas in the two configurations, no RF secondary plasma was generated. The spatial distributions of T_e and n_e in different magnetron configurations were measured, as illustrated in Figure 3.9a. For the balanced dual magnetron, the distributions of the plasma parameters showed some distinct features. First, higher n_e was observed near the center of the magnetron between r = 37 and r = 56 mm, as

shown in the plane z = 0, where n_e increased from 5.6×10^9 ($\pm 4.5\times10^8$) cm^{-3} at r = 0 to a maximum of 1.8×10^{10} ($\pm 1.4\times10^9$) cm^{-3}. Such a profile reflects the plasma shape confined by the balanced magnetron pair which can be seen directly in Figure 2.7. Second, when the probe was moved away from the z = 0 plane, the n_e profile over r was immediately flattened out. Even in the plane of z = 13 mm, the peak could barely be seen. This implies that the plasma is intensively concentrated to the magnetron (target) surface rather than dispersed around. It agrees with the magnetic field distribution in a balanced magnetron pair. Third, as the probe approached the substrate (z = 51 mm), n_e kept decreasing to as low as 6.0×10^9 ($\pm 4.8\times10^8$) cm^{-3}.

A different distribution scenario was observed in the closed-field unbalanced configuration. At the plane of z = 13 mm, an obvious peak point in the n_e profile existed. Compared to the balanced configuration, the peak position was shifted to the right and the value was higher. At z = 51 mm, n_e of the closed-field unbalanced configuration was evenly distributed at about 1.2×10^{10} ($\pm 9.6\times10^8$) cm^{-3}, about twice the density in the balanced configuration. It should be noted that the cathode voltages were different for these two setups even though the current was kept the same (50 mA). The discharge voltage was 205 V for the balanced magnetron and 250 V for the closed-field unbalanced magnetron. The more concentrated plasma to the cathode in the balanced configuration made it easier to maintain the discharge so that the discharge voltage was lower in constant current mode. On the other hand, in a closed-field unbalanced configuration, a larger fraction of plasma was diffused to the substrate, which could provide a higher and more uniform metal flux to a large area of the substrate. In all, the measured n_e profiles in the balanced and closed-field unbalanced magnetron configurations well depict the shapes of the generated plasmas shown in Figure 2.7.

The distribution of T_e was also characterized as shown in Figure 3.9b. T_e was higher in the target region than near the substrate, likely because the magnetic field helps confined the high energy electrons from being quickly lost to the wall. Also, T_e slightly decreased after

switching from the balanced to the closed-field unbalanced configuration and became more uniform over the whole substrate at a farther position (z = 51 mm). Hence in terms of uniformity in T_e, a closed-field unbalanced magnetron pair may provide additional benefits for the thin film deposition on a large substrate.

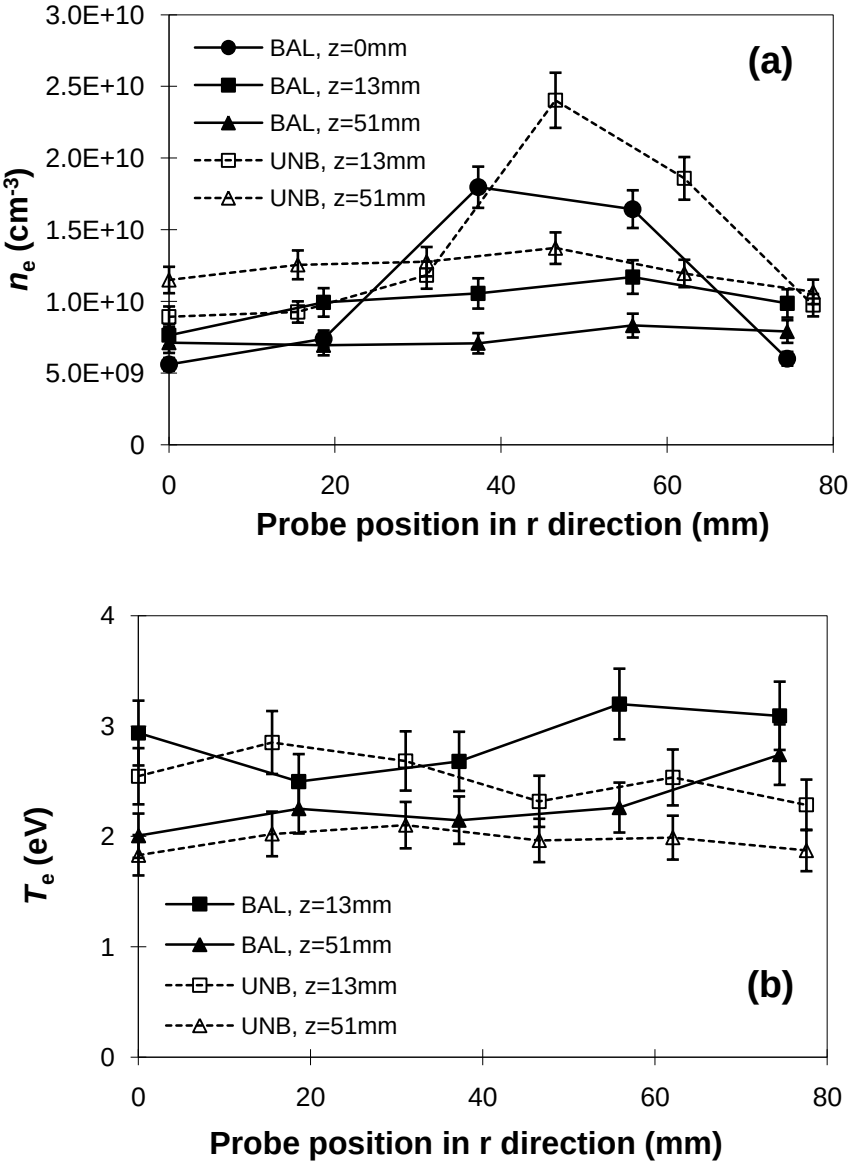

Figure 3.9 Spatial distribution of n_e and T_e of the DC magnetron plasma (without RF enhancement) in different magnetron configurations of balanced ("BAL") and closed-field unbalanced ("UNB"). The gas pressure and electrode current were 5 mTorr and 50 mA per cathode, respectively. Measurements were performed near the magnetron (z=0, 13mm) and near the substrate (z=51mm).

The spatial distributions of the RF enhanced magnetron plasma and the influences of RF power were investigated in both the balanced and closed-field unbalanced magnetron. The same magnetron current of 50 mA and pressure of 5 mTorr as above were used, while a secondary RF power was increased from 0 to 200W. The voltage on the dc magnetron was observed to decrease with the increased RF power (e.g. approximately from 230 to 170V for the closed-field magnetron). The spatial distributions of plasma parameters in the balanced and closed-field unbalanced magnetron are shown in Figure 3.10 and Figure 3.11, respectively. The plasma distributions looked similar in these two configurations. The radial profiles of n_e at both z = 13mm and z = 51mm were enhanced by at least one order of magnitude after applying a 200W RF power. For the balanced magnetron (Figure 3.10a), n_e was higher than that in the closed-field unbalanced configuration (Figure 3.11a). This is understandable since the plasma in the closed-field unbalanced configuration is more diffusive due to its magnetic field shape (as shown in Figure 2.6). Also as mentioned in Section 2.1, the strength of the inner magnets of the closed-field dual magnetron was reduced, which also weakened the plasma confinement. The n_e decreased smoothly over the r direction, which was dominated by the supplemental RF discharge rather than by the DC magnetron discharge. For the T_e at different positions, no obvious effect of RF power was observed. The RF plasma greatly enhanced the electron density, which could further ionize the sputtered metal atoms to facilitate the energy transfer to the film and thus more effective ITO deposition.

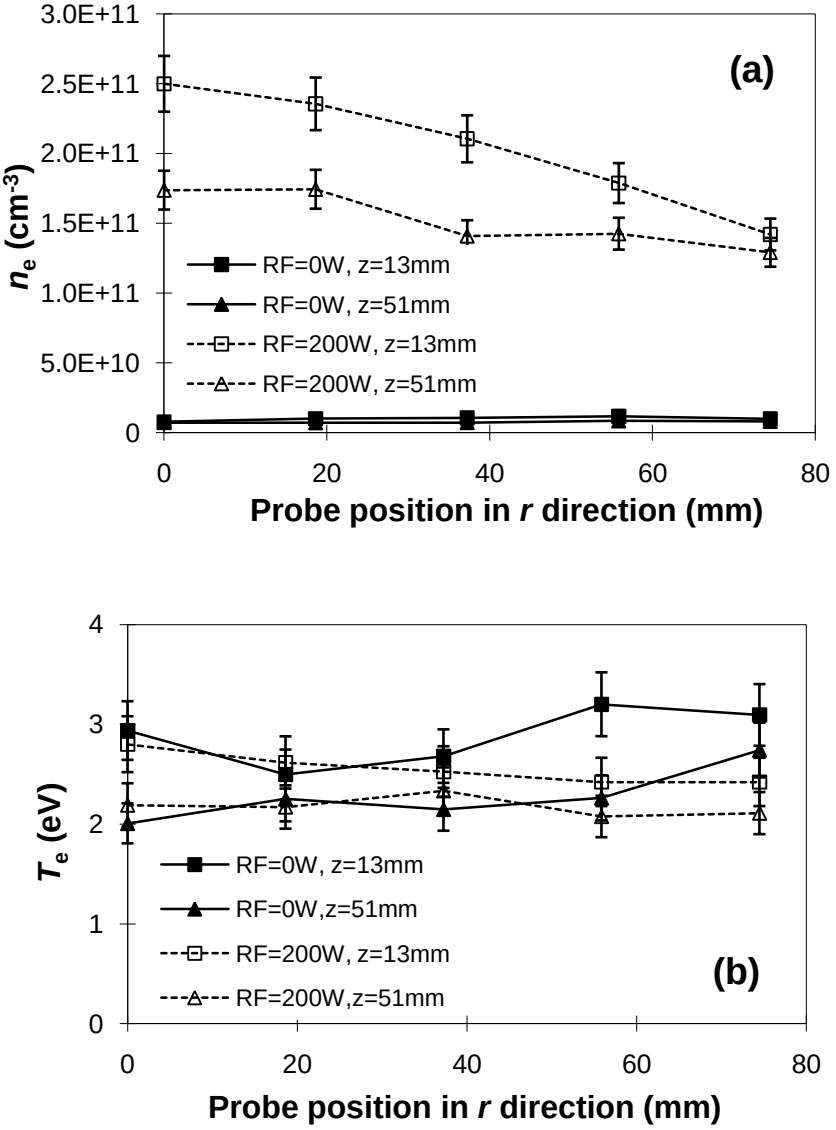

Figure 3.10 (a) Spatial profiles of n_e in the balanced configuration with and without 200W supplemental RF power, (b) the corresponding T_e distribution. The gas pressure and electrode current were 5 mTorr and 50 mA per cathode, respectively. Measured at z=13 mm and z=51 mm.

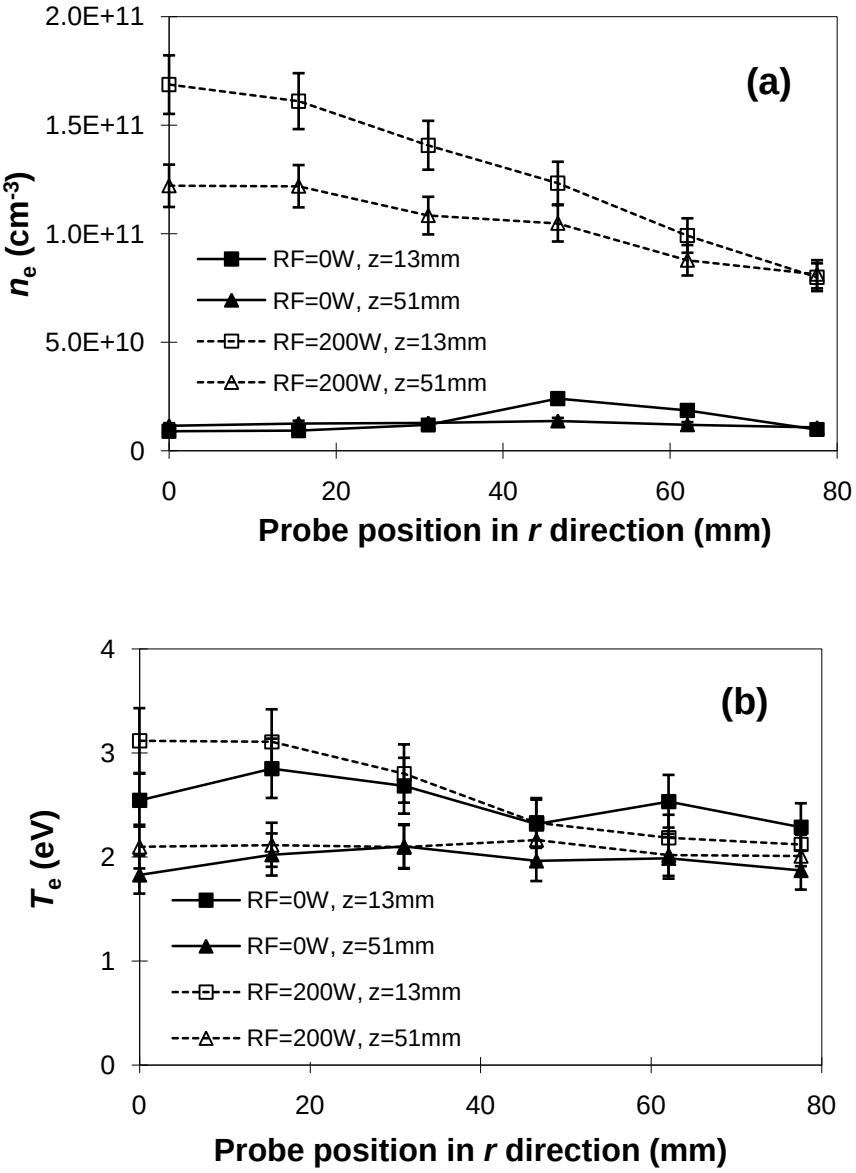

Figure 3.11 (a) Spatial profiles of n_e of the sputtering plasma in the closed-field (unbalanced) configuration with and without supplemental RF assistance. (b) The corresponding T_e distribution. The gas pressure and electrode current were at 5 mTorr, 50 mA per cathode, respectively. Measured at z=13 mm and z=51 mm.

3.4 Chapter Summary

A 3-D scanning RF-compensated Langmuir probe was used for the plasma diagnostics in an RF enhanced dual magnetron. The method used to analyze the probe data including the error analysis was described. A prototype of the 2-inch balanced dual magnetron system with a coupled RF coil was first used to study the influence of RF power, magnetron current and pressure, etc. Applying a secondary RF power of 400 W to a DC magnetron plasma significantly increases n_e to one order of magnitude higher while reducing T_e from about 3 to 2 eV. The electron density also scales with an increasing magnetron discharge current. T_e shoots up initially as a high-voltage magnetron sheath being generated, and decreases when the cathode current further increases. A higher pressure leads to an increased n_e and slightly decreased T_e, which is likely originated from a higher frequency of electron scattering/ionization, and thus more significant energy losses.

Further studies were performed in the 3-inch dual magnetron with ITO targets. Similar effects of RF power and pressure on the plasma were seen. An electron density as high as 10^{12} cm^{-3} was achieved at 400 W RF power, showing a high efficiency of RF coupling. 3-D plasma profiles were measured in both the balanced and closed-field unbalanced magnetron configurations. The comparison showed that the DC magnetron plasma is more concentrated to the targets in the balanced configuration, while in the closed-field unbalanced configuration it is dispersed to the substrate. The plasma profiles agree well with the corresponding magnetic fields and the confined plasma shapes. For a same magnetron current, the closed-field configuration exhibits twice higher plasma density at the substrate region, implying a higher and more uniform metal flux to facilitate a high-rate large area film deposition. For the RF assisted magnetron plasma in both configurations, n_e decreases smoothly over the radial direction, while T_e basically remains constant. In the whole plasma region, electron density is greatly enhanced by the supplemental RF, which should be able to enhance the ionization of the sputtered atoms and benefit the energy transfer to the films and more effective ITO deposition.

Chapter 4 Ionization Fraction Measurements

According to the Langmuir probe diagnostics, the coupled RF power significantly increases the plasma density, which is expected to promote the ionization of sputtered atoms. The plasma also depends on the cathode current, gas pressure and magnetron configuration. It is desirable to directly characterize the ionization faction (*IF*) and explore its dependence on different parameters. In this chapter, a method is described using an assembly of gridded energy analyzer (GEA) and quartz crystal microbalance (QCM). The ionization fractions of the sputtered material were measured at varied RF power, gas pressure and in different magnetron configurations. The investigation not only helps understand the plasma behavior in the RF-enhanced magnetron sputtering, but also provides a criterion for optimizing the process parameters of film deposition.

4.1 Geometrical factor

The concept of GEA/QCM assembly to measure the ionization fraction (*IF*) was introduced in Section 2.3. By measuring the total deposition flux Φ_{tot_QCM} and the neutral flux Φ_{N_QCM}, the ionization fraction could be calculated as

$$IF = \frac{\Phi_{\mathrm{tot\_QCM}} - \Phi_{\mathrm{N\_QCM}}}{\Phi_{\mathrm{tot\_QCM}} - \Phi_{\mathrm{N\_QCM}} + \Phi_{\mathrm{N\_QCM}}/G} \qquad 2.4$$

Here G is a geometrical factor which comes from the shielding of the neutral flux by the GEA side walls, as illustrated in Figure 4.1. A description of the calculation of G was given by Green *et al* [56]. The author used the ratio of flux reaching the entire bottom area of the GEA cylinder to the incidence flux entering its top opening as the geometrical factor G. It depends on the angle distribution of the incoming neutral flux. Two different pressure regimes were considered in related with this distribution. At very low pressure, no collisions happen until the sputtered atoms reach the QCM, so the cosine distribution of atoms from the target surface is maintained. While at very high pressure the neutral flux is close to an isotropic distribution, considering the multiple collisions they run through.

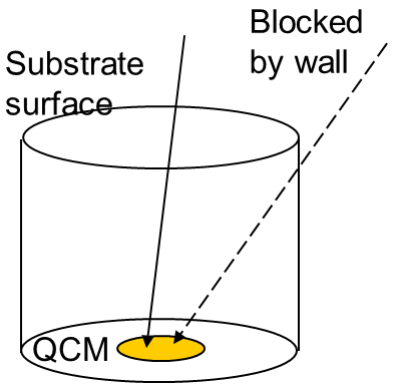

Figure 4.1 The schematic diagram showing the shielding effect of the neutral flux by GEA.

In this thesis, only the deposition on the QCM crystal is concerned, so the calculation of geometrical factor needs to be refined by considering the probability of neutral flux injected onto the QCM crystal surface. For an isotropic distribution of the neutral flux, any point on the bottom can only see the plasma in a certain solid angle instead of 2π on the wafer, so the flux is reduced by the ratio of solid angles. For a point off the center, an integral was done to find this solid angle. For the cylindrical geometry of GEA, denote the radius of the top opening as *R*, the radium of QCM crystal on the bottom surface as *r* and the height as *l*. Then the geometrical factor can be expressed by the following integration over the top surface area and bottom QCM crystal area, divided by $2\pi \cdot \pi r^2$ as the product of solid angle on the top surface and the area of the crystal, as

$$G = \int_0^R \int_0^{2\pi} \int_0^r \int_0^{2\pi} \frac{l}{(l^2 + r_t^2 - 2r_t r_b \cos\theta_b + r_b^2)^{3/2}} r_t d\theta_t dr_t r_b d\theta_b dr_b \cdot \frac{1}{2\pi \cdot \pi r^2} \qquad 4.1$$

where (r_t, θ_t) is a point in cylindrical coordinates on the top surface of the opening and (r_b, θ_b) is a point on the bottom surface. For the GEA we used, the height l = 0.41 inch, top opening R = 0.40 inch and the radius of QCM crystal r = 0.161 inch, giving a calculated G as 0.274.

This G factor calculation is used for the high pressure regime, when the approximation of isotropic distribution of the neutral flux stands. To judge whether the pressure is high enough, the mean free path of particles and the distance between target and QCM should be compared. The mean free path could be calculated as

$$\lambda = \frac{RT}{\sqrt{2}\pi d^2 N_A P} \qquad 4.2$$

where T is the gas temperature (assumed at 300K), d is the diameter of the atom (for Ar, it's 3.48 Å) and P is the pressure. For a normal condition as 10 mTorr, λ=0.578 cm (0.228 inch). The distance between the target and QCM is about 3 inch, which is more than 10 times longer, so many times of collisions exist during the transportation. It should be noted that the realistic distribution of neutrals won't be exactly isotropic, considering there is a net flux from the target to the substrate (QCM) in the chamber. But to a certain extent, the above calculation of G factor as 0.274 can give a close estimation of ionization fraction.

The incident ions are governed by the electric field in the sheath. Since the ion energy is low compared with the sheath drop of about 10V, it can be assumed that the ion flux is perpendicular to the substrate/GEA surface. As a result, the ion flux at the QCM sensor and that at the substrate would be about the same if there were no screens present, and the factor G for ions would simply be unity.

4.2 Ionization fraction of Cu in the 2-inch Magnetron

The ionization fraction measurements were first performed in the 2-inch dual magnetron, in a balanced configuration. Both magnetrons used Cu targets, with the current per cathode ranged between 10 and 50 mA. An RF power up to 300W was applied to the coil to assist the further ionization of metal flux. The Ar pressure was varied between 5 and 40 mTorr.

The functionality of the GEA/QCM assembly was tested first. In a DC magnetron plasma without RF assistance, the QCM recorded the metal deposition rates of the metal flux going through 3 layers of grids under different bottom grid bias in the range of 0 to 60 V. The top grid was floating and the middle grid was biased at -15 V. The detailed grid bias setup of the GEA can be found in Section 2.3. Figure 4.2 shows the results for two conditions of 30 mA and 50 mA per cathode at 10 mTorr. It could be identified that the deposition rate was highest at 0 V bottom bias. It gives a good approximation of the maximum deposition rate, even though more negative bias might slightly increase the deposition rate. This was proved according to some similar experiments (deposition rates vs. bottom grid bias) performed later in the 3-inch magnetron as shown in Figure 4.5, where -10 V or –20V as the bottom bias was used to make sure all the ions are collected. When the bottom bias was increased by 10 V, the deposition rate significantly reduced. Further increasing the bias up to 60 V led to a slowly decreasing rate. The highest deposition rate was correlated to the total flux of metal ions and neutrals which made through the grids and deposited on the QCM sensor. The ion energy in the plasma is usually much lower, comparing with the electron energy of several eV, so when the bottom grid was set at several volts higher than the plasma potential, most of ions were repelled back leading to a greatly reduced deposition rate. A very small portion of ions with higher energies were further eliminated by higher bottom biases. To a good approximation, +30V almost repelled all the ions and allowed only neutral atoms to the QCM sensor. Such a test verified that the GEA/QCM assembly worked properly and gave the reasonable results.

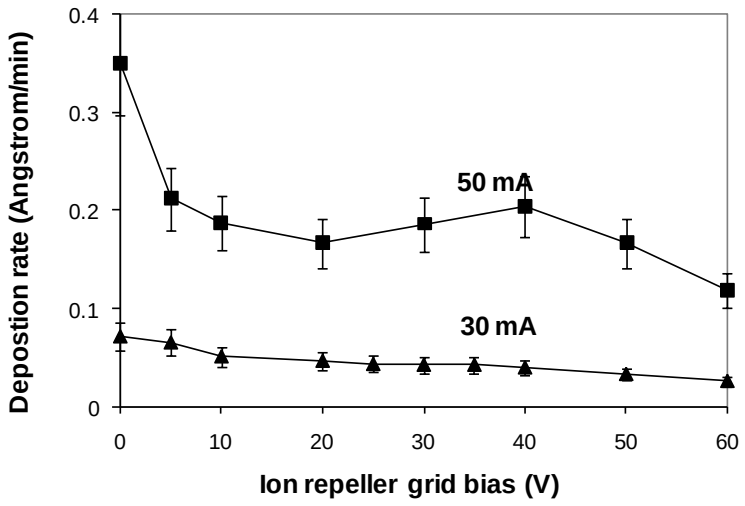

Figure 4.2 Deposition rate as a function of bias on the ion repeller grid. Cu targets, cathode currents of 30 mA and 50 mA respectively, 10 mTorr, no RF assistance.

The effect of RF assistance on the ionization of Cu flux was studied. The magnetron was operated at 30 mA per cathode and 10 mTorr, when the RF power was increased from 0 to 300W. The deposition rates under an ion repeller grid bias of 0V and 50 V were recorded respectively, as displayed in Figure 4.3. The top curve represents the total flux of Cu ions and neutrals on the QCM sensor with 0V bias, while the lower curve consists of neutral flux only. Both the rates increased with the RF power, however, not in direct proportion. This point could be seen more clearly after calculating the ionization fraction using Equ. 2.4. Figure 4.4 shows the Cu ionization fractions at different RF power input. In order to see the effect of geometrical factor, G=1 and G=0.274 are used individually for the calculation. The selection of geometrical factor directly affects the *IF*, e.g., the *IF* under 300W RF assistance changes from 73% to 43% when G=0.274 is applied. However, the trends are still the same, namely that ionization fraction increases with the RF assistance. The calibrated *IF* increases from 15 to 43% with the RF power increased from 0 to 300W, which is as expected and provides a solid reason for the observed RF promotion of the ITO film deposition as shown in the next chapter.

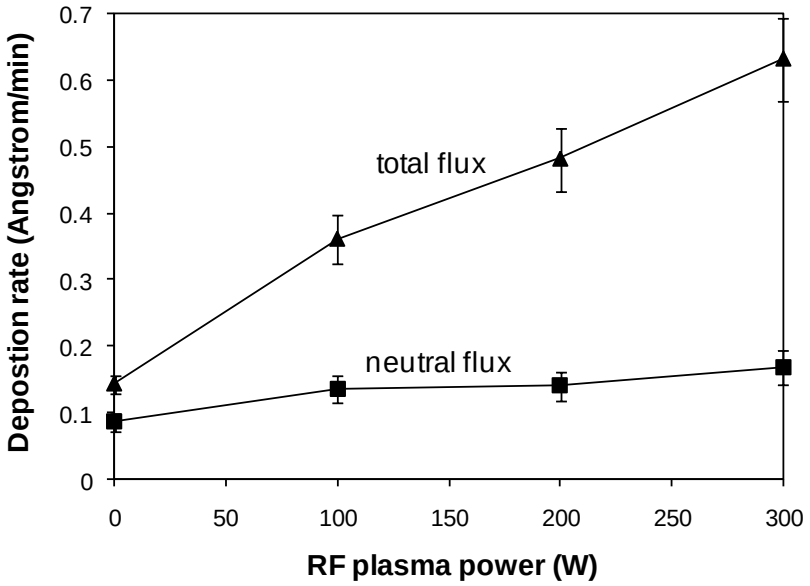

Figure 4.3 The effects of RF power on the deposition rates of total flux (bottom bias=0V) and of neutral flux itself (bottom bias=50V) on the QCM sensor. Cu targets, 30 mA per cathode, 10 mTorr.

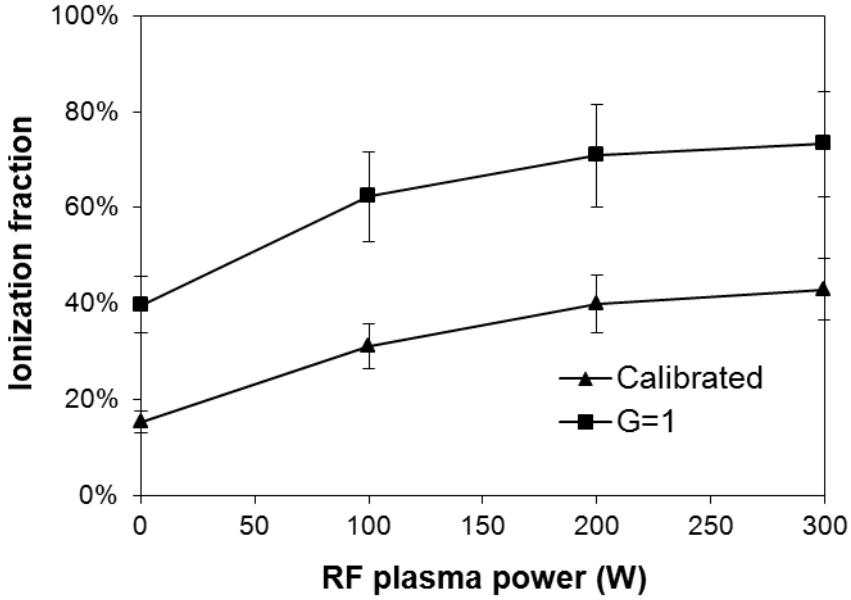

Figure 4.4 The dependence of ionization fraction (*IF*) on the assisting RF power (calibrated with G=0.274). Cu targets, cathode currents of 30 mA, 10 mTorr. As a comparison, the ionization fractions without calibration (assuming G=1) are also given.

4.3 Ionization Fraction of ITO in the 3-inch Magnetron

After the preliminary tests in the 2-inch magnetron with Cu targets, ionization fractions were further measured in the 3-inch dual magnetron using ITO targets. Both the balanced and closed-field configurations were studied and compared to each other. The magnetron discharge was run at 50 mA per cathode and in 5 mTorr Ar. For the GEA operation, as mentioned previously in Section 4.2, -10 V or -20 V as the lowest bottom bias was used to collect all the ions. The deposition rates at different bottom biases were recorded. The measurements in the balanced mirrored configuration under different RF power between 0 and 200 W are shown in Figure 4.5 (a). As the bottom bias was decreased to -10 V, the deposition rate basically saturated, implying that all the ions were collected. As the bias increased up to +50 V, the deposition rate on the QCM reduced and gradually flattened out so that only neutral flux deposited on the QCM crystal. It was also noticed that the total deposition rate was enhanced by higher RF input power, which is an important advantage for the film deposition process. Similar results have also been obtained for the unbalanced closed-field magnetron, as shown in Figure 4.5 (b).

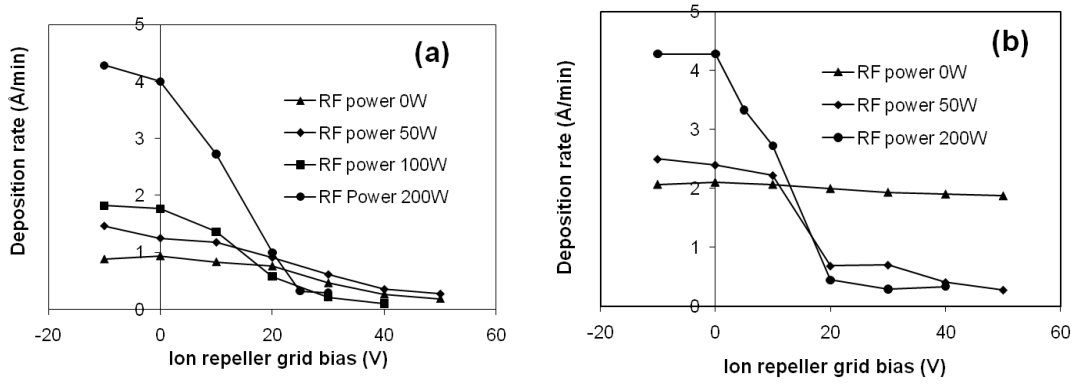

Figure 4.5 Deposition rate on the QCM crystal as a function of bias on the ion repeller grid. ITO targets, 50 mA per cathode, 5 mTorr, 0-200 W RF power. (a) For balanced dual magnetron, (b) for closed-field (unbalanced) dual magnetron.

Based on these measurements, the ionization fraction was calculated for various RF power input. Isotropic neutral flux model was assumed for the calibration. *IF* in balanced and closed-field magnetron configurations are compared in Figure 4.6. In the balanced configuration, *IF* increased from 39% to 78% as RF power increased from 0 to 200W. After

the magnetron being switched to the closed-field configuration, *IF* was reduced. Especially in the case without RF assistance, a dramatic decrease of *IF* from 39% to 5% was seen. The plasma in the balanced magnetron was more concentrated to the cathode surface. As a result, the sputtered metal atoms were ionized more intensively and effectively. As mentioned in Section 2.1, the stronger magnets in the balanced magnetron pair and thus a better plasma confinement also contributed to a higher ionization fraction in the balanced magnetron configuration. This low *IF* in the closed-field magnetron configuration could be compensated by additional RF power. 200W RF power increased the ionization fraction to 76%, almost the same as in the balanced dual magnetron. This was because the incorporated RF secondary plasma provided denser electrons in the whole region. It should be noted that our measurements were performed near the substrate level rather than near the target. A substantial fraction of neutral atoms are scattered out of the plasma and are lost to the chamber wall, while ions are better confined in the plasma. This gives a higher ion fraction near the substrate than near the target. Anyway, the RF coil significantly enhanced the ionization of target materials to about 80%, no matter what magnetron configuration was used. It is very likely for the film quality to be improved by the RF assistance in magnetron configurations.

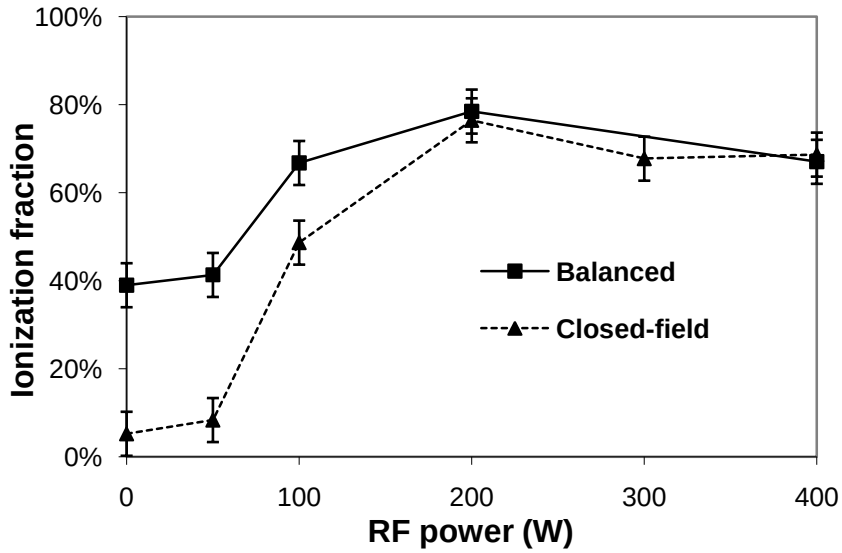

Figure 4.6 Ionization fraction measured in different magnetron configurations and at different RF power. 5 mTorr, 50 mA per cathode, RF power from 0 to 400 W.

Further experiments were conducted to find the effect of gas pressure on the ionization fraction. No RF was introduced to distinguish this effect. As shown in Figure 4.7, *IF* increases with the pressure as a general trend. A maximum of ionization fraction at the middle-range pressure of 5-10 mTorr (around 1 Pa) exists for both configurations. At a lower pressure, the mean free path of the particles is so large that the ionization of sputtered material is inefficient. At a higher pressure, increased scattering reduces electron energies and consequently the ionization cross section. This confirms the above measurements that the balanced magnetron generates higher *IF* than the closed-field magnetron, especially at the low pressure range (<5 mTorr). As the pressure further increases, too frequent collisions make the plasma distributions in the two configurations less distinctive. The electron temperature dominates the ionization process that the ionization fractions become comparable.

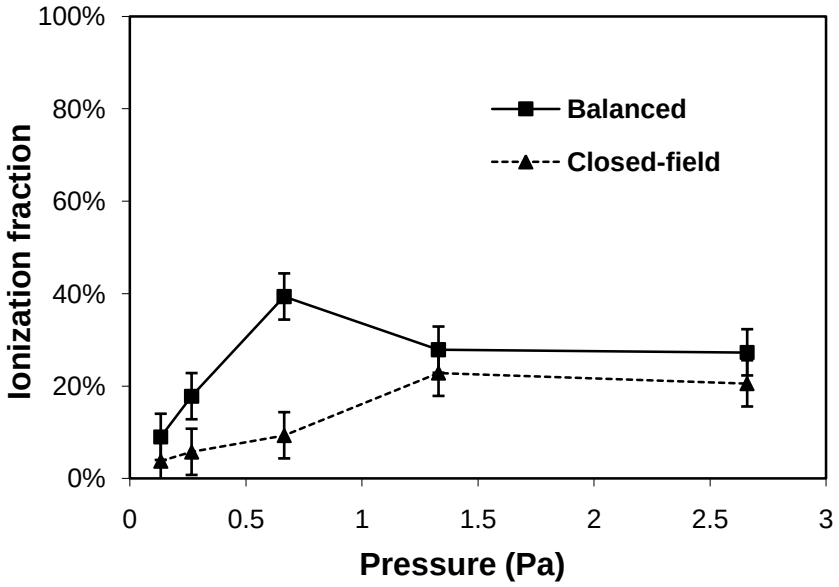

Figure 4.7 Effect of pressure on the ionization fraction, 1-20 mTorr, 50 mA per cathode, No additional RF input.

4.4 Chapter Summary

Ionization fractions of the sputtered flux in the RF-assisted dual magnetron were measured using a suite of 3-layer gridded energy analyzer (GEA) to admit or repel the ion flux, combined with a quartz crystal microbalance (QCM) to record the corresponding deposition rates. Appropriate grid biases of the GEA were determined experimentally. The top grid was floating and the middle grid was biased at -15 V. The bottom grid was set at -10V and 50 V to get the total deposition rate and the neutral flux deposition rate, respectively. The effect of shielding the neutral flux by the GEA side walls was considered and a refined method to find an appropriate geometrical factor G was used. The ionization fractions of sputtered flux were determined for both the 2-inch and 3-inch dual magnetron.

In the 2-inch dual balanced magnetron with Cu targets, both the neutral flux and the ion flux increases with RF power. The Cu ionization fraction increases from 15 to 43% as the RF power increases from 0 to 300W. For the 3-inch magnetron (with ITO targets), the effect of the magnetron configuration was investigated. Without an RF assistance, the balanced configuration has a much higher ionization than the closed-field configuration, namely 39% vs. 5%. This difference originates from the more concentrated plasma in the vicinity of the target which ionizes the metal atoms more effectively, as compared to the diffusive plasma in the closed-field configuration. In this sense, the balanced magnetron is superior for ITO film deposition since more ion species are demanded. However, the ionization fraction can be greatly enhanced by the supplemental RF power. For example, 200W RF assistance increases the ionization fraction from 5% to 76% in the closed-field configuration, which is almost identical to the 78% in the balanced dual magnetron mode with the same RF power. Appropriate RF assistance is crucial to achieve a high ionization fraction, not matter which magnetron configuration is used. The pressure also affects the ionization fraction, showing a maximum at 5-10 mTorr for both magnetron configurations. The longer mean free path at a lower pressure and the reduced electron energy at a higher pressure suppress the ionization process.

Chapter 5 ITO Film Deposition

Indium tin oxide (ITO) films were fabricated on both glass and polyethylene terephthalate (PET) substrates in the RF-enhanced closed-field magnetron system, without using substrate heating or post-processing. Among various process parameters, the secondary RF power was specially investigated in related to the electrical conductivity and the optical transmission of the films. The film stoichiometry was determined by X-ray photoelectron spectroscopy (XPS). Atomic Force Microscopy (AFM) was employed to further characterize the surface morphology of the ITO films in order to study its correlation with the film properties. The prototype system was later adapted for a large area roll-to-roll deposition system using dual 3.5×18 inch linear magnetron cathodes. ITO films were deposited on large area PET substrates, and initial efforts were made to optimize the film properties by applying an appropriate assisting RF power.

5.1 ITO Deposition in the Closed-field Magnetron

The previous diagnostics have shown various advantages of the RF enhanced closed-field dual magnetron. The magnetron plasma density is higher and more uniform near the substrate, which is suitable for a large-area film deposition. RF enhancement gives an increased ionization fraction of sputtered atoms. This is promising with a potential of producing high quality ITO films at a relatively low substrate temperature. For the following experiments, ITO films were deposited using the 3-inch closed-field dual magnetron. The correlations between the ITO film properties and the process parameters such as the RF power were studied. In the future, ITO films should also be fabricated in the balanced mirrored configuration to compare with the results from the closed-field dual magnetron.

The ITO deposition procedure has been described in Section 2.4. It involves different controlling parameters, such as the cathode current, gas pressure, O_2/Ar ratio, RF power, and deposition time. It would be time-consuming to test each of them. For the preliminary

investigation, the effect of RF power was focused on while the other parameters were fixed at some "probably good" values from literatures. The cathode current was set at 90 mA (the power supply was limited to 100 mA), pressure at 5 mTorr, O_2/Ar at approximately 2% (limited by the accuracy of mass flow controllers), with deposition time of 45 minutes to get 300 to 400 nm thick films. The substrate was floating instead of being negatively biased.

Before ITO films deposition, the influence of the RF power on the magnetron discharge characteristics were measured first (Figure 5.1). As the RF power was increased from 0 to 300 W, the DC voltage decreased from 258 to 189 V to get a constant magnetron current of 90 mA . The secondary RF plasma contributes some electron and ion currents to the DC magnetron discharge, consequently lowering the discharge voltage.

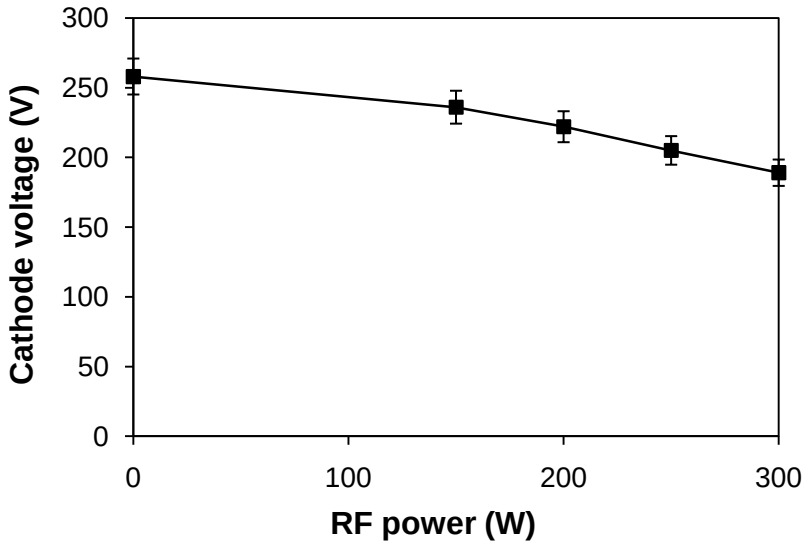

Figure 5.1 The DC voltage on the magnetron with different RF assistance. The cathode current was maintained at 90 mA during discharge.

Using the closed-field configuration, depositions of ITO films were made on both glass and PET substrates, as described in Section 2.4. Deposition rates were measured based on the thickness measurements from a profilometer (Dektak 3030). As shown in Figure 5.2, the deposition rate decreased from 16.4 to 5.4 nm/min as the RF power was increased from 0 to 300 W. Since the magnetron current was kept constant, the change could only be due to the variation of voltage. As the voltage decreases, the sputtering yield of the target decreases

correspondingly, i.e. the flux of ITO atoms reduces.

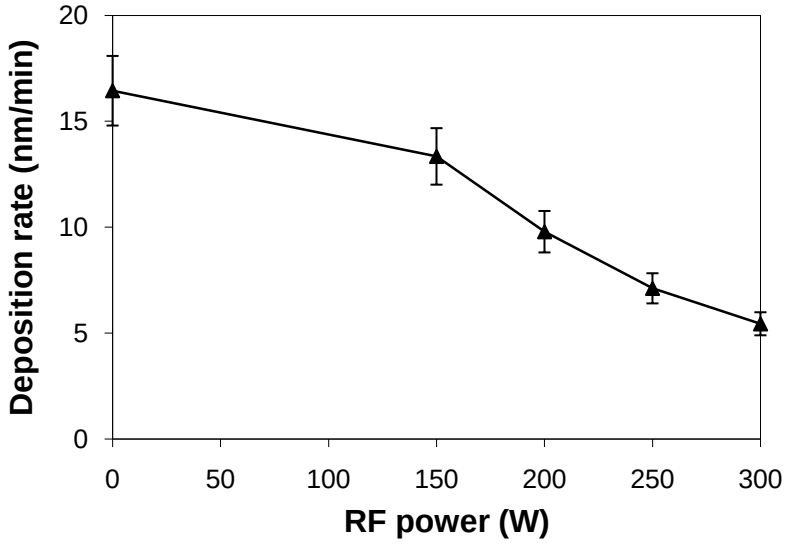

Figure 5.2 Deposition rates of ITO films, measured using profilometry.

Figure 5.3 shows the influence of the secondary RF power on the electrical resistivity of the ITO films and the average optical transmittance in the visible spectrum (340–650 nm). Here the bulk resistivity of the film was calculated as a product of the film thickness and the sheet resistance measured from a four point probe. It turned out that at 150W or below, barely no conductivity (very high resistivity of 4×10^{-1} Ohm-cm) was identified on either glass or PET samples. Such a result is not surprising. As mentioned in Section 1.1, the ITO films typically require an elevated substrate temperature and post-annealing processes to improve the conductivity. For a conventional DC magnetron sputtering, the as-deposited ITO films before annealing normally have a high resistivity as in the range of 10^{-1} and 10^{-3} Ohm-cm [9,10]. In our case, the high resistivity could also be caused by the empirically chosen process parameters such as O_2/Ar ratio and pressure. They usually significantly affect the electrical properties [60-62,63] and need further optimization. Fortunately, this doesn't hinder us from seeing the effects of coupled RF power on the ITO film qualities.

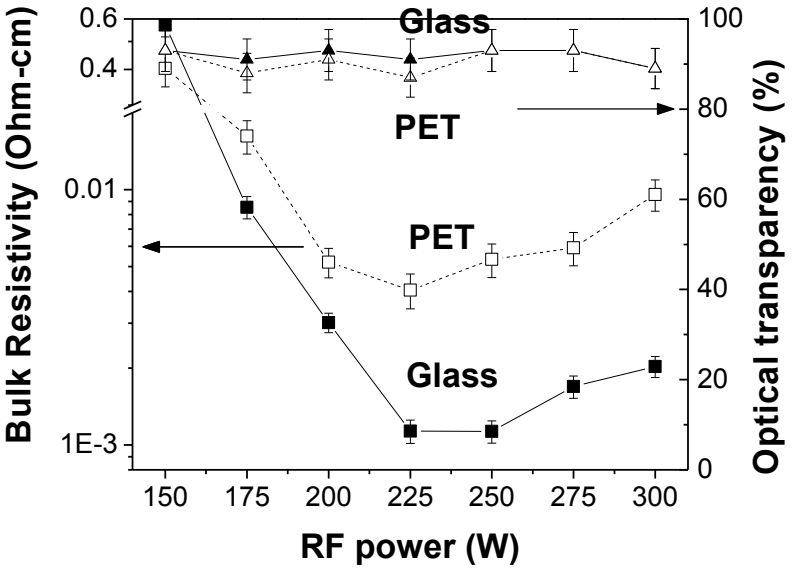

Figure 5.3 The bulk resistivity and optical transparency of the ITO films deposited under different auxiliary RF powers. The depositions were performed at 5 mTorr, 2% of O_2 in Ar, 90 mA cathode current while RF power was varied between 150 and 300 W.

By applying an RF power of about 225-250 W, the film resistivity was significantly reduced from 4×10^{-1} Ohm-cm to 1.2×10^{-3} Ohm-cm on the glass substrate, after which resistivity began to increase again. The glass samples deposited at 150W, 225W and 300 W of RF power were chosen for further characterizations and their electrical and optical properties were compared in Table 5.1. The lowest sheet resistance was achieved at 225 W, with a sheet resistance of 30 Ohm/sq and the corresponding bulk resistivity of 1.1×10^{-3} Ohm-cm. Meanwhile, the optical transmittance of the film did not show a large variation, basically above 91% for the glass sample and above 87% for the PET. During the deposition process the substrate temperature was monitored, and shown to increase with a higher RF power (Figure 5.4). For 225 W, the substrate temperature was well kept below 110 ℃, which is suitable for a variety of organic substrates. The experiment results confirm the clear trend that assisting RF power can increase the conductivity dramatically. Actually the electrical properties here may be further improved. The bulk resistivity was higher than 5×10^{-1} Ohm-cm without RF assistance, as contracted to a typical reported resistivity lower than 10^{-3} Ohm-cm using magnetron sputtering only [64]. Experiments should be performed, for example to optimize the O_2 content and pressure, and remove the diagnostic tools to achieve a cleaner

chamber environment.

Table 5.1. Properties of the films deposited at 150, 225 and 300W. Here the thicknesses were measured by a profilometer.

RF Power (W)	Cathode current (mA)	Substrate temperature (℃)	Thickness (nm)	Sheet resistance (Ohm/square)	Resistivity (Ohm-cm)	Optical transmittance (%)
150	90	66	347	16500	5.7×10^{-1}	93%
225	90	110	378	30	1.1×10^{-3}	91%
300	90	127	356	57	2.0×10^{-3}	89%

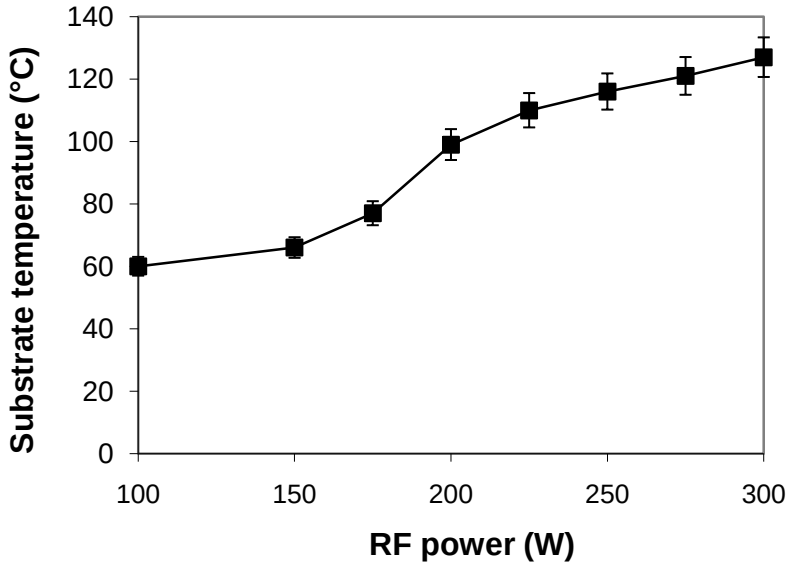

Figure 5.4 The substrate temperature at varied input RF power.

It is known that in the conventional methods of preparing ITO film, the deposition usually requires a high enough substrate temperature to achieve good film properties [8-9,12,65]. The RF secondary plasma is used here as an effective alternative approach to provide additional energy to the growing films. Due to the existence of RF plasma, more $Ar+O_2$ ions and metal ions are generated. It has been demonstrated that ionization fraction increases at higher RF power. These ions, after being accelerated by the plasma potential, can deposit their energies to the substrate and thus promote the ITO growth. This explains why the film deposited at 225 W had a higher conductivity than that deposited at 150 W. Another important factor to affect the film conductivity might be the oxygen vacancies in the ITO film. It has been widely observed that the oxygen partial pressure can significantly affect the ITO

film resistivity [60-62]. Even though the ITO evaporation source itself has the stoichiometric oxygen content in the material, oxygen deficient films were obtained with no or low additional oxygen flux conditions, exhibiting a high resistance and a low optical transmittance. Additional oxygen is necessary to increase the oxygen ion beam flux and thus increase the oxygen incorporation into the oxygen-deficient ITO film, which will reduce the resistivity by compensating for too high oxygen vacancies in the film. However, an excessive oxygen flow will decrease oxygen vacancies in the film more than the required amount and again resulting in an increase in the resistivity [60]. In our setup, even though the oxygen partial pressure was fixed, the oxygen ion flux could be increased by the additional RF plasma. It turned out that RF power of 225 W (or 250 W) generates the most appropriate oxygen ion flux, to get the lowest resistivity of the film, and a higher RF assistance power (e.g. 300 W) won't further increase the electrical conductivity.

5.2 Film Characterization

The stoichiometry of the ITO films was determined with the XPS. Figure 5.5 shows the typical survey spectra of the samples. The peaks of In, Sn, and O were detected as expected. For ITO films deposited at different conditions, XPS showed consistent results that they have almost identical spectra. A contamination of stainless steel (judged from the Ni, Fe elements) appeared in the film, which is likely due to the etching of the dark space shield of the magnetron source or the RF coil (even though it was covered with the fiber tape). Such a contamination issue might degrade the film quality and should be addressed in the future.

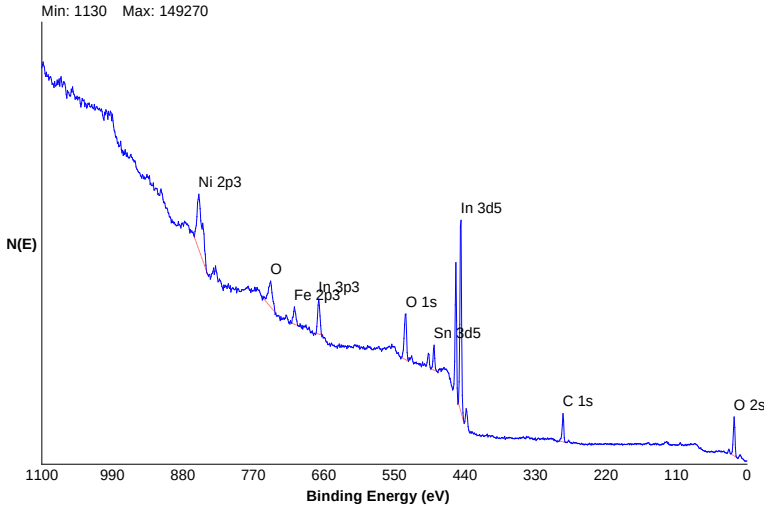

Figure 5.5 XPS survey spectra of the ITO film deposited on glass in RF-assisted closed-field magnetron system.

High resolution scanning of the In 3d5, Sn 3d5 and O 1s peaks was used to determine the atomic compositions of each element. Results for the three samples produced under different RF power are listed in Table 5.2. The one using 225 W RF enhancement has atomic compositions of 34.3% In, 3.7% Sn and 62.0% O, which agree well with the predicted target composition of 90% In_2O_3 and 10% SnO_2 by weight. A calculation shows that the ITO stoichiometry should be 35.6% : 3.6% : 60.7% for In : Sn : O. As the RF power increases, the O content increases and becomes slightly above the stoichiometric value, which supports the above explanation of the improvement of film conductivity due to RF enhanced oxygen

incorporation.

Table 5.2 The atomic composition of the ITO films deposited under different RF enhancement (150, 225, and 300W). Other conditions are 90 mA current per cathode, 5 mTorr, 2% O_2 in Ar, 45 min deposition.

Sample	Atomic composition		
	In	Sn	O
#1 (150W)	36.2%	4.0%	59.8%
#2 (225W)	34.3%	3.7%	62.0%
#3 (300W)	33.4%	3.9%	62.7%

The AFM images revealed that samples deposited at different RF powers exhibited distinct surface morphologies, as shown in Figure 5.6. The sample deposited at 150 W RF showed the roughest surface with a root mean square (RMS) roughness of 3.3 nm with large grains on it. For 225 W, the RMS roughness of surface was reduced to 0.9 nm and the grains were much finer. Lee [66] has reported a surface roughness of 0.7 nm for an indium zinc oxide (IZO) thin film using an ion-assisted deposition system. He attributed this to the enhanced surface mobility of adatoms by ion bombardment. Our result was close to Lee's and was lower than most typical reported values around 1-2.5 nm [20,22]. The sample of 300 W RF revealed a similar surface morphology as the 225 W RF sample, with an RMS roughness of 1.1 nm. Basically, the smoothness of the film surface was improved and the grain sizes became smaller with an increased RF power. This is especially important for the applications of ITO films to the organic light emitting diodes (OLEDs) or other opto-electronic devices.

The promotion of oxygen ionization by RF assistance may also contribute to the smaller grain sizes at a higher RF power. More oxygen is incorporated in the films on interstitial lattice sites, which hampers the grain growth due to the formation of more grain boundaries, dynamic incorporation and segregation of oxygen during deposition [60,67].

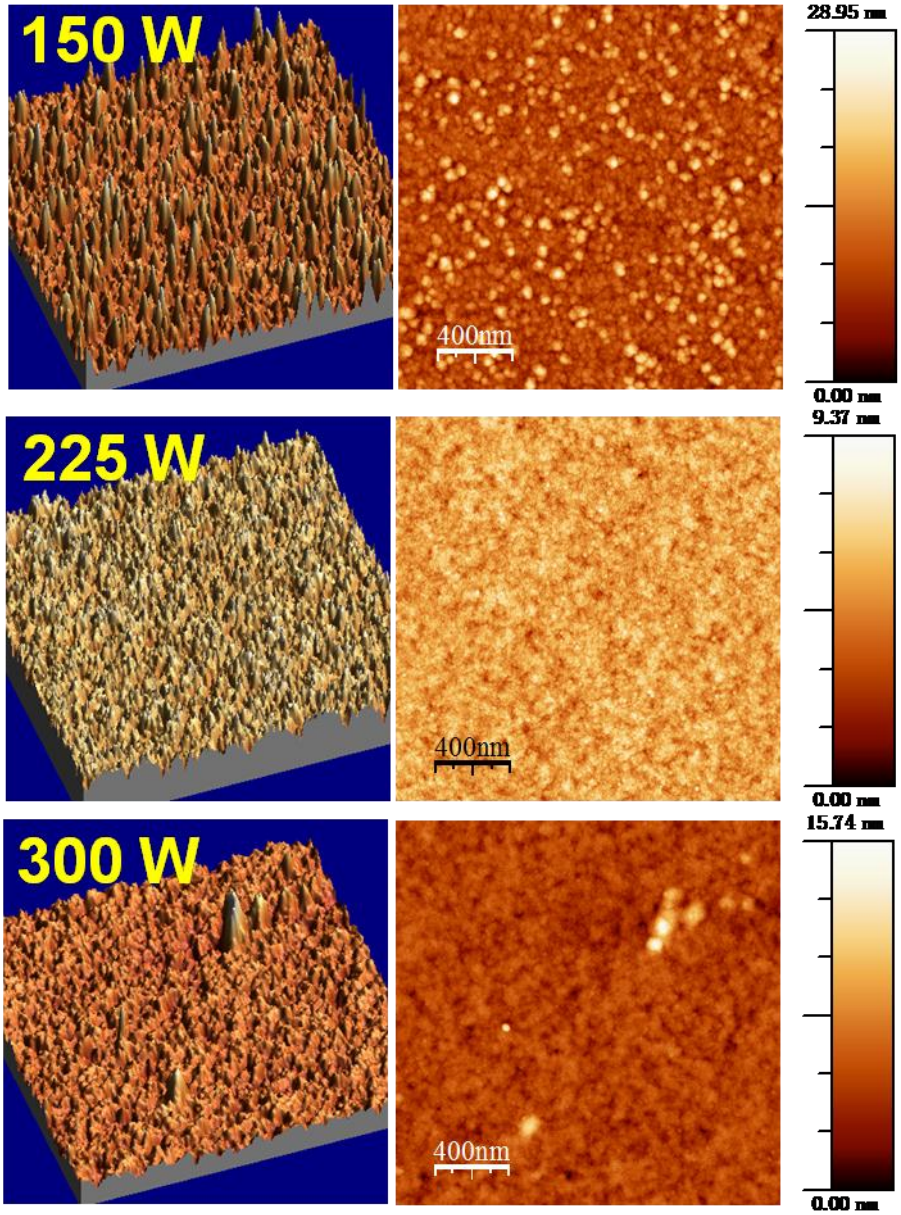

Figure 5.6 AFM scans of the films deposited at the different auxiliary RF power conditions from 150 to 300 W.

5.3 Deposition on Large-area Substrates

Trial runs were made to deposit ITO films on the polyethylene terephthalate (PET), using a dual 3.5×18 inch linear magnetron tool designed for large-area substrates. The details of the device and experiments have been described in Section 2.4. By varying different processing parameters, ITO films with thicknesses range between 250 and 400 nm were achieved after a constant deposition time of 10 min. The base pressure was 2×10^{-5} Torr before deposition. Secondary RF power was varied from 0 to 400W and some other parameters were fixed such as 0.8 A cathode current, 5 mTorr gas pressure, and 0% O_2/Ar ratio. Figure 5.7 shows the electrical resistivity of ITO films under different RF power enhancement. The bulk resistivity was reduced when applying a higher RF power. At 300W RF, a minimum resistivity of 3.4×10^{-3} Ohm-cm with a transparency of 90% was obtained on PET. Further increasing the RF power to 400W resulted in an abrupt increase of resistivity. This trend is similar as obtained in the smaller scale (3-inch magnetron) system. Again, the RF enhancement was attributed to the more efficient energy transfer and oxygen incorporation into the film. The deposition rates were measured in a range of 23 to 31 nm/min on the plastic substrates when 100 to 400 W RF was applied, with the highest rate obtained at 300 W RF. The enhanced deposition rates than those in the 3-inch magnetron were due to the much larger target dimensions.

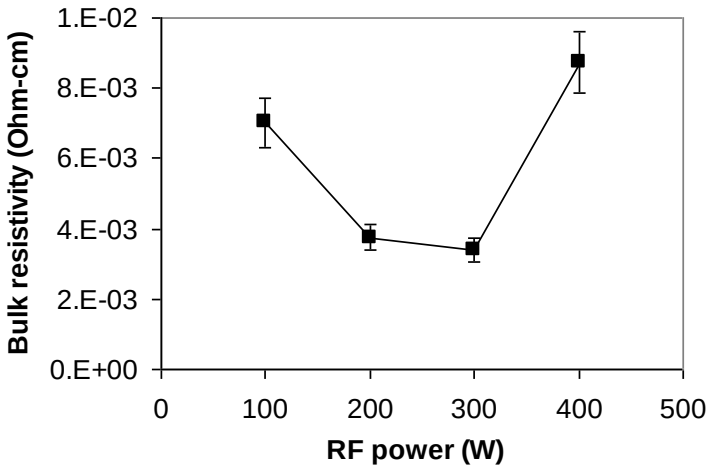

Figure 5.7 Influence of RF power on the resistivity of ITO film on PET substrate, at 0.8 A of cathode current, 5 mTorr of Ar and base pressure of 2×10^{-5} Torr.

The substrate temperature was monitored during the entire processes (Figure 5.8). It increased rapidly at the beginning of processes and gradually flattens out. Under various conditions tested, the temperature during the processes was always below 130 ^{o}C, which makes the system suitable for many applications using the PET substrates.

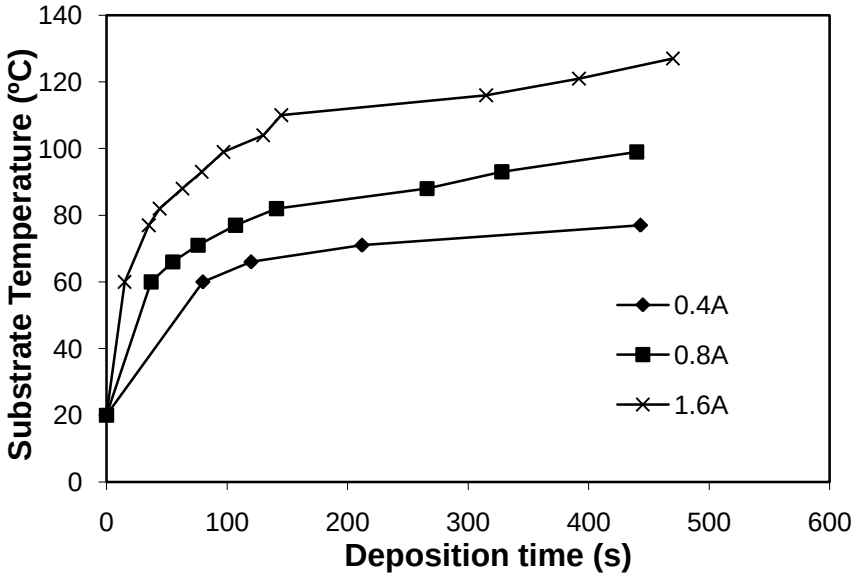

Figure 5.8 Temperature evolution during the film deposition process. Different magnetron current was used and RF power was fixed at 300W.

By increasing the magnetron current to 1.6 A and adjusting the ratio of O_2 to Ar gas flow to 0.5%, an ITO film of 520nm was achieved with 300 W RF assistance after 10 min. The deposition rate was substantially increased to 52 nm/min. The bulk resistivity was lowered to 1.4×10^{-3} Ohm-cm and the transparency in the visible light range was 89%. The substrate temperature went up to 127 ℃ in the 10-min deposition process as shown in Figure 5.8. However, in order to get a thickness of 150nm to satisfy the typical industrial requirements, only 3 min was necessary to keep the temperature below 110 ℃.

In all, a substantial increase of the film conductivity was achieved in the RF assisted DC magnetron, which is feasible for a large-area, high-rate and low-temperature deposition of ITO or other function materials. Further improvements can be made by adjusting the pressure, tuning the O_2/Ar ratio and utilizing the closed-field magnetron configuration, etc., to meet the industrial requirement of a resistivity between 10^{-3} and 10^{-4} Ohm-cm.

5.4 Chapter Summary

Indium tin oxide (ITO) films were deposited on both glass and polyethylene terephthalate (PET) substrates in the RF-assisted closed-field 3-inch dual magnetron system at low substrate temperatures. As a critical parameter to enhance the ionization, the supplemental RF power was studied with regard to the electrical resistivity and optical transmittance of the ITO films. It was observed to dramatically improve the film conductivity by two orders of magnitude. An optimum film with a low resistivity of 1.1×10^{-3} Ω-cm and a visible light transmittance of 91% was achieved using 225 W RF; meanwhile the substrate temperature was maintained below 110 ℃. The enhanced ions flux by the secondary RF plasma directly deposits energy to the substrate after being accelerated by the plasma sheath, promoting the ITO growth. The RF plasma also ionizes more O_2 so that oxygen becomes more effectively incorporated into the ITO film, which compensates a large amount of oxygen vacancies in the film to greatly increase the film conductivity. X-ray photoelectron spectroscopy (XPS) confirmed the ITO film stoichiometry, with a slightly higher oxygen content. Atomic Force Microscope (AFM) revealed that the surface roughness of the films was greatly reduced to 0.9 nm with an RF assistance of 225 W, probably due to an enhanced mobility of adatoms on the substrate surface by the increased bombardments of ion flux. The low roughness the fabricated ITO films makes them suitable for many applications in opto-electronics.

The RF-assisted dual magnetron prototype has been extended to a larger rectangular linear dual-magnetron designed for a flat panel display manufacturing system. ITO films were fabricated on large-area PET substrates, while a similar improvement of film properties by auxiliary RF was observed. A bulk resistivity of 1.4×10^{-3} Ω-cm and an optical transmittance of 89% were achieved with 300W RF. The system enabled significant rates of 23-52 nm/min while maintaining a substrate temperature below 130 ℃. A broader study of various process parameters other than the secondary RF power should be performed to further improve ITO film qualities.

Chapter 6 Conclusions

In this work, an innovative RF-coupled closed-field dual magnetron sputtering system was developed, for the purpose of large-area deposition of indium tin oxide (ITO) films among various transparent conductive oxides at low substrate temperatures without the need for post-annealing processes. I performed both plasma diagnostics and ITO films deposition to explore the merits of such a system and to understand the effects of different parameters on the plasma environments and film qualities. The Langmuir probe measurements of the electron density and temperature revealed a great enhancement of plasma intensity by the coupled RF power and a superiority of the closed-field (unbalanced) magnetron configuration. The RF plasma also significantly increased the ionization fraction of target materials, as determined using a gridded energy analyzer (GEA) and a quartz crystal microbalance (QCM). ITO films were fabricated on both glass and polyethylene terephthalate (PET) at low substrate temperatures, and an obvious improvement of the film conductivity was achieved by the RF assistance.

The system consists of dual 3-inch DC magnetrons which can be operated at either a mirror (balanced) configuration or a closed-field (unbalanced) configuration. An RF coil was fabricated and placed between the two magnetron cathodes to initiate a strong secondary plasma, with the applied power up to 500W. The closed-field configuration creates a plasma in the intervening area, which is extended further to the substrate rather than being confined near the target. The secondary RF plasma enhances the ionization of the sputtered atoms. The ion flux efficiently deposits energy to the growing films and produced high quality ITO films at a low substrate temperature without additional substrate heating and post-annealing, which is critical for the ITO applications using organic substrates.

RF-compensated Langmuir probe, as a simple and powerful measure to achieve the information of the plasma, was employed to study the influences of individual process parameters. It helps optimize the parameter set and understand the correlations between the

plasma conditions and film properties. For this work, I constructed a 3-D Langmuir probe to measure the spatial distributions of electron density n_e and electron temperature T_e of the plasma. The balanced and closed-field configurations were compared with each other. The n_e profiles of the DC magnetron plasma reflect the distinct shapes of two magnetic field configurations. In the balanced configuration, the plasma is intensively concentrated to the magnetron/target surface. In the closed-field configuration it is diffused to the substrate giving a twice higher plasma density at the substrate region, implying a higher and more uniform metal flux to facilitate a high-rate film deposition on large area substrates. When the RF power was applied (up to 400 W), electron temperature slightly decreased from 3.2 to 2.8 eV. And n_e was increased by two orders of magnitude to 10^{12} cm^{-3}, which can enhance the ionization of the sputtered atoms. An increasing gas pressure also affects the plasma by increasing n_e and slightly reducing T_e. A higher pressure implies a higher rate of electron scattering and thus more significant energy losses.

For the RF-coupled closed-field dual magnetron, one critical parameter of sputtering plasma is the ionization fraction of the sputtered atoms. It is desirable to quantitatively study the enhancement of ionization fraction by the new system. For this purpose, I used a gridded energy analyzer (GEA) in conjunction with a quartz crystal microbalance (QCM) to directly measure the ionization fraction. The shielding effect of the non-directional neutral flux by the GEA casing walls was considered to calibrate the ionization fraction. The influences of the RF power, magnetron configuration and ambient gas pressure on the ionization fraction were investigated. The mirror (balanced) configuration gives a higher ionization fraction of ITO as 39% as compared to 5% in the closed-field configuration. The lower ionization fraction in the latter is because of a more diffusive plasma and the reduced magnetic field. This deficiency can be compensated by applying a supplemental RF power. In the closed-field configuration, the presence of 200W RF plasma increased the ionization fraction from 5% without RF to 76%, comparable to 78% (increased from 39%) in the balanced configuration. The ionization fraction also varied with the pressure, with a maximum observed at around 5-10 mTorr. The study of ionization fraction facilitates further understanding the plasma behaviors in the

RF-assisted magnetron sputtering, and provides a criterion for optimizing the film deposition process parameters.

The Langmuir probe diagnostics showed a virtue of the closed-field configuration being suitable for large-area depositions; meanwhile, the secondary RF power significantly enhanced the plasma intensity and the ionization of sputtered species. With these promising results, I performed the deposition of indium tin oxide (ITO) films in the closed-field dual magnetron configuration with different RF assistances. Both glass and plastic (PET) substrates were used, and the temperature of substrate was monitored during the deposition. The supplemental RF power was studied in terms of its effect on the film resistivity and optical transmission transparency. It dramatically improved the film conductivity with the other parameters fixed (90 mA cathode current, 5 mTorr, 2% of O_2 in Ar). An optimum film with a low resistivity as 1.1×10^{-3} Ω-cm and a good visible light transmittance as 91% was achieved at 225 W RF. The substrate temperature was below 110℃, enabling ITO films deposition on various organic substrates. We believed that the higher ions flux generated by the secondary RF plasma directly deposit energy to the substrate after being accelerated by the plasma potential and hence promote the ITO growth. It is also likely that the RF plasma ionizes more O_2 so that oxygen can be more efficiently incorporated into the ITO film, compensating a large amount of oxygen vacancies and increasing the film conductivity. The X-ray photoelectron spectroscopy (XPS) confirmed that the oxygen content in the as-deposited ITO films increased with the RF power and slightly exceeded the stoichiometric value in the ITO target. Meanwhile, Atomic Force Microscopy (AFM) was used to study the surface morphologies. The surface roughness was reduced greatly with the RF assistance, due to an enhanced mobility of adatoms or adsorbed molecules on the substrate surface by increased bombardments of ion flux. The low roughness the fabricated ITO films makes them favorable for many applications in opto-electronics.

Finally, I extended the prototype of our 3-inch RF-assisted dual magnetron to a larger rectangular linear dual magnetron in a flat panel display manufacturing system. The initial

experiments were performed to fabricate the ITO films on the large-area PET substrates. A similar improvement of the film properties by the auxiliary RF was observed. ITO films with a bulk resistivity of 1.4×10^{-3} Ω-cm and an optical transmittance of 89% were achieved at 300W RF power. The system enabled significant deposition rate in a range of 23-52 nm/min while maintaining a substrate temperature below 130 ℃. Various process parameters other than the secondary RF power should be investigated to further improve the ITO film qualities.

Chapter 7 Future work

In this thesis, the concept of the RF-assisted closed-field dual magnetron is studied in different aspects. This new configuration shows a great potential to obtain ITO and other transparent conductive oxide films without elevated substrate temperature or extra annealing post-processing steps. High quality ITO films have been obtained at low substrate temperatures on the large area plastic substrates at relatively high deposition rates. However, it should be noted is that there are still many details yet to explore, which can lead to further improvements of the tool design and enhanced film qualities. In this chapter, some investigations proposed for future are discussed.

In order to apply ITO films to industrial applications, the electrical resistivity is generally required to be of order of 10^{-4} Ohm-cm. A refined optimization of the whole set of the process parameters should be performed to lower the film resistivity. As mentioned in Section 5.1, the ITO film deposition procedure involves different controlling parameters. The above studies were focused on the effect of RF power, while the other parameters were only fixed at some "probably good" values due to the time constraints. For example, the pressure was set at 5 mTorr, and the O_2/Ar ratio was approximately 2% which was limited by the accuracy of mass flow controllers. The pressure has been shown to considerably affect the ionization fraction of the sputtered species which plays an important role in the film growth. The O_2/Ar ratio determines the oxygen incorporation into the ITO film, significantly altering the electrical and optical properties. By carefully examining the pressure and O_2 percentage in the gas, the film conductivity is expected to be further increased.

In terms of the ITO film quality, another factor requires attention. According to the X-ray diffraction (XPS), there are impurities of stainless steel in the films. The contamination may come from the etching of the dark space shield surrounding the magnetron cathode or the RF coil (even though it was covered with the fiber tapes). Samples fabricated with and without the secondary RF should be compared using XPS surveys, to verify these

assumptions. In the current design, the RF coil is very close to the dark space shield so that the strong RF plasma may sputter the shield. The RF coil should be repositioned to see if the impurities can be suppressed. To eliminate the sputtering of the RF coil, multiple methods are proposed. A different value of the block capacitor (as shown in Figure 2.4) may reduce the bias on the coil and thus mitigate the issue. Or the coil can be pre-coated with ITO (or other materials difficult to sputter) so that the sputtering won't affect the film composition. A new idea for the RF coil design may also work. Instead of putting a coil in the vacuum chamber, a quartz tube can be used to separate the coil in the atmosphere from the magnetron inside the chamber. An RF plasma can still be generated (as in an inductively coupled plasma) adjacent to the magnetron, while no sputtering of coil gets into the ITO films in this case.

The film should be synthesized in a mirrored balanced configuration to compare with the closed-field dual magnetron case. Based on the plasma diagnostics and ionization fraction measurements, the balanced configuration confines the plasma very close to the surface of the magnetron. This makes it difficult to deposit films on a large area substrate uniformly. However, the concentrated plasma does produce higher ionization. It would be interesting and useful to see if the mirrored balanced configuration produces better ITO films than the closed-field magnetron, with the same RF assistance or even without any RF. The uniformity problem can always be solved by roll-to-roll process.

Eventually, the deposition process should be extended to different materials. The scarcity of indium makes ITO more and more expensive now and various substitute materials have been studied, among which Al-doped ZnO (AZO) shows promising properties as ITO. The RF-assisted closed-field (or mirrored balanced) magnetron should be employed for the AZO films deposition without heating the substrates or annealing the films. The RF power and other process parameters will be tuned to optimize the film qualities.

References

[1] S. A. Bashar, *Study of Indium Tin Oxide (ITO) for Novel Optoelectronic Devices*, PhD thesis, University of London, Department of Electrical Engineering, 1998.

[2] C. W. Tang and S. A. Vanslyke, *Appl. Phys. Lett.* **51**, 913 (1987).

[3] G. Li, C. W. Chu, V. Shrotriya, J. Huang, and Y. Yang, *Appl. Phys. Lett.* **88**, 253503 (2006).

[4] Y. Suzuki, F. Niino, and K. Katoh, *J. Non-Cryst. Solids* **218**, 30 (1997).

[5] K. W. Whang and J. K. Kim, *J. Display Tech.* **1**, 295 (2005).

[6] M. Boehme and C. Charton, *Surf. Coat. Technol.* **200**, 932 (2005).

[7] B. Lucas, W. Rammal, and A. Moliton, *Eur. Phys. J. Appl. Phys.* **34**, 179 (2006).

[8] R. X. Wang, C. D. Beling, S. Fung, A. B. Djurišić, C. C. Ling, and S. Li, *J. Appl. Phys.* **97**, 033504 (2005).

[9] I. H. Yang, Y. Lee, J. N. Jang, and M. Hong, *Thin Solid Films* **517**, 4165, (2009)

[10] L. Lin, F. Lai, Y. Qu, R. Gai, and Z. Huang, *Mater. Sci. Eng. B* **138**, 166 (2007)

[11] L. -J. Meng and F. Placido, *Surf. Coat. Technol.* **166**, 44 (2003)

[12] Y. Hu, X. Diao, C. Wang, W. Hao, and T. Wang, *Vacuum* **75**, 183 (2004).

[13] J. M. Blocher Jr., *Thin Solid Films* , 51(1981).

[14] D. H. Zhang, H. L. Ma, P. Ma, S. Z. Win, and S. Y. Li, *Thin Solis Films* **263**, 105 (1995).

[15] M. Fujinaka and A. A. Berezin, *Thin Solid Films* **101**, 10 (1983).

[16] R. Pommier, C. Gril, and J. Maruchhi, *Thin Solid Films* , 91 (1981).

[17] J. Machet, J. Guille, P. Saulnier, S. Robert, *Thin Solid Films* **80**, 149 (1981).

[18] C. M. Dai, C.S. Su, and D.S. Chuu, *Appl. Phys. Lett.* 57, 1879 (1990).

[19] S. Laux, N. Kaiser, A. Zoller, R. Gotzelmann, H. Lauth, and H. Bernitzki, *Thin Solid Films* **335**, 1 (1998).

[20] C. Liu, T. Matsutani, T. Asanuma, M. Kiuchi, E. Alves, and M. Reis, *Nucl. Instrum. Methods Phys. Res.* B **206**, 348 (2003).

[21] Y. Han, D. Kim, J. S. Cho, and S. K. Koh, *Thin Solid Films* **473**, 218 (2005).

[22] D. Kim, *Vacuum* **81**, 279 (2006).

[23] F. O. Adurodija, H. Izumi, and T. Ishihara, *Vacuum* **59**, 641 (2000).

[24] D. Kim and S. Kim, *J. Vac. Sci. Technol.* A **20**, 1314 (2002).

[25] S. L. Liao, L. S. Hung, W. C. Chan, X. M. Ding, T. K. Sham, I. Bello, C. S. Lee, and S. T. Lee, *Appl. Phys. Lett.* **75**, 1619 (1999).

[26] T. Minami, *Thin Solid Films* **516**, 5822 (2008)

[27] S. Berg and T. Nyberg, *Thin Solid Films*, **476**, 215 (2005).

[28] N. Li, J. P. Allain, and D. N. Ruzic, *Surf. Coat. Technol.* **149**, 161 (2002).

[29] A. Matthews, *J. Vac. Sci. Technol. A* **21**, S224 (2003).

[30] D. R. Gibson, I. Brinkley, E. M. Wadell, and J. M. Walls, *Proc. SPIE Int. Soc. Opt. Eng.* **7101**, 710108 (2008).

[31] J. A. Hopwood, *Ionized Physical Vapor deposition*, Academic Press, 2000.

[32] *The International Technology Roadmap for Semiconductors*, Semiconductor Industry Association (2007), http://public.itrs.net.

[33] S. M. Rossnagel, *Semicond. Int.* **21**, 99 (1996).

[34] I. Hashim, V. Pavate, D. Peijun, B. Chin, D. Brown, and T. Nogami, *Proc. SPIE Int. Soc. Opt. Eng.*

3508, 58 (1998).

[35] B. Narayanan, C. Y. Li, L. Kangsoo, Y. Bo, W. J. Jie, P. D. Foo, and J. Xie, *Proc. SPIE Int. Soc. Opt. Eng.* **3883**, 42 (1999).

[36] M. Yamashita, *J. Vac. Sci. Technol. A* **7**, 151 (1989).

[37] S. M. Rossnagel, and J. Hopwood, *J. Vac. Sci. Technol. B* **12**, 449 (1994).

[38] T. Ono, C. Takahashi, and S. Matsuo, *Jpn. J. Appl. Phys.* **23**, L534 (1984).

[39] C. Doughty, S. M. Gorbatkin, T. Y. Tsui, G. M. Pharr, and D. L. Medlin, *J. Vac. Sci. Technol. A* **15**, 2623 (1997).

[40] L. Meng, R. Raju, R. Flauta, H. Shin, D. N. Ruzic, and D. B. Hayden. *J. Vac. Sci. Technol. A* **28**, 112 (2010).

[41] L. C. Yang, G. S. Chen, and A. Rockett, *Appl. Phys. Lett.* **86**, 1 (2005).

[42] J. N. Kim, H. Y. Lee, D. K. Lee, and J. J. Lee, *Surf. Coat. Technol.* **201**, 5442 (2007).

[43] David N. Ruzic. *Electric Probes for Low Temperature Plasmas.* AVS Press, New York, 1994.

[44] I. D. Sudit and F. F. Chen. *Plasma Sources Sci. Technol.* **3**, 162 (1994).

[45] V. A. Godyak, R. B. Piejak, and B. M. Alexandrovich, *Plasma Sources Sci. Technol.* **1**, 36 (1992).

[46] D. R. Juliano, *Modeling and Measurements of An Ionized Physical Vapor Deposition Device Plasma*, PhD thesis, University of Illinois-Urbana, Department of Nuclear Engineering, 1999.

[47] P. Horowitz and W. Hill, *The Art of Electronics*. Cambridge University Press, New York, second edition, 1989 , p. 32.

[48] D. R. Juliano, D. N. Ruzic, M. M. C. Allain, and D. B. Hayden, *J. Appl. Phys.* **91**, 605 (2002).

[49] A. Sankaran and M. J. Kushner, *J. Vac. Sci. Technol. A* **22**, 1242 (2004).

[50] V. Vyas and M. J. Kushner, *J. Vac. Sci. Technol. A* 24, 1955 (2006).

[51] J. E. Foster, W. W. Wang, A. E. Wendt, J. H. Booske, *IEEE International Conference on Plasma Science*, p 223 (1998).

[52] K. Okimura, and T. Nakamura, *J. Vac. Sci. Technol. A* **21**, 988 (2003).

[53] I. Petrov, A. Myers, J. E. Greene, and J. R. Abelson, *J. Vac. Sci. Technol. A* 12, 2846 (1994).

[54] Z. H. Barber, C. Christou, K. -F. Chiu, and A. Garg, *Vacuum* **69**, 53 (2002).

[55] S. M. Rossnagel and J. Hopwood, *Appl. Phys. Lett.* **63**, 3285 (1993).

[56] K. M. Green, D. B. Hayden, D. R. Juliano, and D. N. Ruzic, *Rev. Sci. Instrum.* **68**, 4555 (1997).

[57] D. B. Hayden, D. R. Juliano, M. N. Neumann, M. C. Allain, and D. N. Ruzic, *Surf. Coat. Tech.* **120-121**, 401 (1999).

[58] C. Bohm, and J. Perrin, *Rev. Sci. Instrum.* **64**, 31 (1993).

[59] R. Raju, L. Meng, R. Flauta, H. Shin, M. J. Neumann, T. A. Dockstader, and D. N. Ruzic. *Plasma Sources Sci. Technol.* **19**, 025011 (2010).

[60] Y. S. Kim, Y. C. Park, S. G. Ansari, J. Y. Lee, B. S. Lee, and H. S. Shin, *Surf. Coat. Technol.* **173** 299 (2003).

[61] J. W. Bae, H. J. Kim, J. S. Kim, N. E. Lee, and G. Y. Yeom, *Vacuum* **56**, (2000).

[62] S. N. Luo, A. Kono, N. Nouchi, and F. Shoji, *J. Appl. Phys.* **100**, 113701 (2006).

[63] P. Canhola, N. Martins, L. Raniero, S. Pereira, E. Fortunato, I. Ferreira, and R. Martins, *Thin Solid Films* **487**, 271 (2005)

[64] F. Kurdesau, G. Khripunov, A. F. da Cunha, M. Kaelin, and A. N. Tiwari, *J. Non-Cryst. Solids* **352**, 1466 (2006).

[65] A. Ray, R. Banerjee, N. Basu, A. K. Batabyal, and A. K. Barua, *J. Appl. Phys.* 54,3497 (1983).

[66] W. J. Lee, *Solid State Electron.* **46**, 4 **(**2002).

[67] D. Mergel, W. Stass, G. Ehl, and D. Barthel, *J. Appl. Phys.* **88**, 2437 **(**2000).

AUTHOR'S BIOGRAPHY

Liang Meng was born on July 23, 1984 in Suzhou, Anhui, China. He attended the Department of Modern Physics at University of Science and Technology of China (USTC) in 2000. During the 4 years of college study, he became interested in plasma physics and engineering. Liang received his Bachelor of Science degree in Applied Physics in July 2004 and decided to continue a graduate study in Plasma Physics at USTC. For the next three years he worked as a research assistant in the Low Temperature Plasma Laboratory, before he completed a Master of Science degree in Plasma Physics from USTC in July 2007. In order to achieve more advanced knowledge in USA, Liang applied for the Department of Nuclear, Plasma, and Radiological Engineering, at University of Illinois at Urbana-Champaign. After the admission, he joined the Center for Plasma-Material Interactions led by Prof. David N. Ruzic in August 2007. He will receive a M.S. degree in Nuclear, Plasma, and Radiological Engineering in December of 2010 and will continue to pursue for a Ph.D. degree.